HHS Public Access

Author manuscript

Nat Immunol. Author manuscript; available in PMC 2025 January 22.

Published in final edited form as:

Nat Immunol. 2023 December ; 24(12): 2032–2041. doi:10.1038/s41590-023-01671-2.

CD47 masks pro-phagocytic ligands in *cis* on tumor cells to suppress anti-tumor immunity

Zhenghai Tang[1], **Ming-Chao Zhong**[1], **Jin Qian**[1], **Cristian Camilo Galindo**[1,2], **Dominique Davidson**[1], **Jiaxin Li**[1,2], **Yunlong Zhao**[3], **Enfu Hui**[3], **André Veillette**[1,2,4,*]

[1]Laboratory of Molecular Oncology, Institut de recherches cliniques de Montréal (IRCM), Montréal, Québec, Canada H2W1R7;

[2]Department of Medicine, McGill University, Montréal, Québec, Canada H3G 1Y6;

[3]Department of Cell and Developmental Biology, School of Biological Sciences, University of California San Diego, La Jolla, CA 92093;

[4]Department of Medicine, University of Montréal, Montréal, Québec, Canada, H3T 1J4

Summary

Cancer cells often overexpress CD47, which triggers the inhibitory receptor SIRPα expressed on macrophages, to elude phagocytosis and anti-tumor immunity. Pharmacological blockade of CD47 or SIRPα is showing promise as anti-cancer therapy, although CD47 blockade has been associated with hematological toxicities that may reflect its broad expression pattern on normal cells. Herein, we found that, in addition to triggering SIRPα, CD47 suppressed phagocytosis by a SIRPα-independent mechanism. This mechanism prevented phagocytosis initiated by the pro-phagocytic ligand, SLAMF7, on tumor cells, due to a *cis* interaction between CD47 and SLAMF7. The CD47-SLAMF7 interaction was disrupted by CD47 blockade, as well as by a first-in-class agonistic anti-SLAMF7 antibody, but not by SIRPα blockade, thereby promoting anti-tumor immunity. Hence, CD47 suppresses phagocytosis not only by engaging SIRPα, but also by masking cell-intrinsic pro-phagocytic ligands on tumor cells. This previously unsuspected mechanism may influence deciding between CD47 blockade or SIRPα blockade for therapeutic purposes.

Keywords

anti-tumor immunity; immunotherapy; immune checkpoints; phagocytosis; macrophages; CD47; SIRPα; SLAMF7

*Correspondence: andre.veillette@ircm.qc.ca.

Author contributions

Z.T., M.C.-Z., J.Q., D.D., Y.Z., E.H. and A.V. designed experiments. Z.T., M.C.-Z., J.Q., C.C.G., J.L. and Y.Z. performed experiments. All authors interpreted the results. Z.T. and A.V. wrote the manuscript. All authors commented on the manuscript. A.V. and E.H. provided funding.

Competing interests

The authors will file a patent on the use of MAb Z10 for the treatment of SLAMF7-positive human tumors. They declare no other competing interests.

Introduction

Therapeutic blockade of inhibitory immune checkpoints has been one of the most significant recent advances in anti-cancer treatment[1, 2]. Monoclonal antibodies (MAbs) blocking inhibitory receptors expressed on T cells (such as CTLA-4 and PD-1) or their ligands have shown significant efficacy against a wide range of cancer types and have been approved for patient care. However, these agents are not effective against many cancers. This limitation prompted researchers to evaluate other inhibitory immune checkpoints as candidates, including receptors expressed on innate immune cells[3–9]. Macrophages, as well as other phagocytes like neutrophils, are amongst the most primitive components of the immune system[4, 6, 10]. The main functions of macrophages are phagocytosis leading to destruction of other cells, cytokine production and antigen presentation to T cells. Consequently, they can be highly effective in anti-tumor immunity.

The activation of macrophages is controlled by the balance between the engagement of activating and inhibitory cell surface receptors, by ligands expressed or not on potential “target” cells. When activating receptors are predominantly triggered, macrophages are activated and display effector functions. The macrophage activating receptors include receptors for the Fc portion of antibodies (FcRs), the apoptotic cell receptor MerTK, the integrin CD11b (Mac-1) and the homotypic receptor SLAMF7[5, 8, 10, 11]. However, when inhibitory receptors are predominantly triggered, macrophage activation is suppressed. The best-studied macrophage inhibitory receptor is signal inhibitory regulatory protein (SIRP) α, which recognizes as ligand CD47 that is expressed of nearly all normal cells and is often overexpressed on tumor cells[3, 4, 8, 9].

There has been increasing interest in blocking the SIRPα-CD47 immune checkpoint to promote phagocytosis and anti-tumor immunity[5–7, 10, 12, 13]. Blockade of the SIRPα-CD47 interaction, by anti-CD47 MAbs, anti-SIRPα antibodies or soluble SIRPα-Fc fusion proteins, has shown promising results as anti-cancer immunotherapy in pre-clinical studies and phase 1 clinical trials, in particular against hematological malignancies[5–7, 13, 14]. The ability of SIRPα-CD47 blockade to augment phagocytosis also requires co-engagement of activating receptors, such as FcRs or SLAMF7, by ligands on tumor cells[3–5, 8, 10, 15].

FcRs are engaged when tumor-opsonizing antibodies, such as the therapeutic anti-CD20 MAb rituximab, are present[6, 10, 11]. In contrast, the homotypic receptor SLAMF7 (the ligand of SLAMF7 is another SLAMF7 molecule expressed on another cell) is engaged when tumor cells, in addition to macrophages, express SLAMF7. In tumors, SLAMF7 is primarily expressed on hematopoietic cancer cells, such as multiple myeloma cells and lymphoma cells[4, 5, 15, 16]. A recent report documented that SLAMF7-negative tumor cells, such as breast cancer cells, can also be artificially decorated with SLAMF7 using bispecific nanoconjugates, to unleash SLAMF7-dependent phagocytosis and anti-tumor immunity[17]. Conversely, the crucial role of SLAMF7 in phagocytosis can be bypassed by inflammatory stimuli, due to activation of unconventional pro-phagocytic integrins CD11a and CD11c[15].

One of the limitations of SIRPα-CD47 blockade has been that agents blocking CD47 also frequently depleted red blood cells and platelets, leading to anemia and thrombocytopenia,

whereas, in one study, agents blocking SIRPα depleted neutrophils, thus causing neutropenia[3, 7, 18–20]. Although the mechanisms involved in these toxicities remain to be clarified, in the case of anti-SIRPα antibodies, neutropenia was attenuated by the use of agents unable to engage FcRs. In this light, one possibility is that the "Fc-intact" SIRPα-CD47 blocking agents trigger FcR-mediated elimination of normal hematopoietic cells expressing CD47 or SIRPα. Another possibility is that the blocking agents have yet unappreciated mechanisms of action that interfere with normal hematopoietic cell homeostasis.

Herein, we found that, in addition to triggering SIRPα, CD47 suppressed phagocytosis and anti-tumor immunity by a SIRPα-independent mechanism. This mechanism was the result of a *cis* interaction between CD47 and SLAMF7 on tumor cells, thus preventing the homotypic *trans* interaction of SLAMF7 on tumor cells with SLAMF7 on macrophages. The CD47-SLAMF7 interaction was disrupted by blockade of CD47, but not of SIRPα, and by a new first-in-class agonistic anti-SLAMF7 antibody. The inhibitory impact of the CD47-SLAMF7 interaction was bypassed when tumor-opsonizing antibodies were present. Hence, CD47 on tumor cells suppresses phagocytosis not only by engaging SIRPα on macrophages, but also by masking tumor cell-intrinsic pro-phagocytic ligands. This divergence of mechanism should be considered when deciding between blockade of CD47 or SIRPα in therapeutic settings.

Results

Blockade of CD47, but not of SIRPα, promotes phagocytosis via SLAMF7

To compare the impact of SIRPα and CD47 on phagocytosis, we evaluated side-by-side the effects of previously described or newly generated blocking anti-CD47 MAbs, blocking anti-SIRPα MAbs, or blocking SIRPα fusion proteins (the latter act by occupying CD47 on tumor cells) (Extended Data Fig. 1a–g). Given the potential deleterious effects of sustained engagement of FcRs and the growing tendency to use MAbs and fusion proteins unable to bind FcRs in the clinic, unless antibody-dependent cellular cytotoxicity or antibody-dependent cellular phagocytosis (ADCP) is attempted[21, 22], all agents were engineered to be "Fc-silent" by mutations in their Fc portion ("LALAPG" mutations) (Extended Data Fig. 1a,b)[23]. These mutations fully abrogated the ability of MAbs to bind FcRs on macrophages (Extended Data Fig. 1b).

When wild-type mouse bone marrow-derived macrophages (BMDMs) were used as phagocytes, blocking anti-mouse CD47 MAb Miap301 augmented phagocytosis of mouse tumor cell lines L1210 (leukemia), P815 (mastocytoma) and SP2/0 (multiple myeloma) *in vitro*, compared to control MAb MOPC21 (Fig. 1a–c). However, no increase in phagocytosis was seen with blocking anti-mouse SIRPα MAbs #23 and #27, which were generated in our laboratory (Fig. 1c and Extended Data Fig. 1c–e). Anti-CD47 MAbs, but not anti-SIRPα MAbs, promoted phagocytosis of normal activated mouse T cells, which can also be phagocytosed during CD47 blockade[5] (Fig. 1d). These observations were made either with microscopy-based or with pHrodo-based phagocytosis assays (Fig. 1a–d and Extended Data Fig. 2a,b). Similar results were obtained when anti-CD47 MAbs were added only to target

cells or anti-SIRPα MAbs were added only to BMDMs, followed by extensive washing to remove unbound antibodies, prior to the phagocytosis assay (Extended Data Fig. 2c,d).

The ability of anti-CD47 MAbs to trigger phagocytosis of L1210 and activated T cells was abolished when BMDMs lacked SLAMF7 or when T cells lacked SLAMF7, confirming the involvement of the homotypic receptor SLAMF7 in this process[5] (Fig. 1e,f). SLAMF7 KO macrophages were already reported to display unaltered FcR-mediated phagocytosis of tumor cells[5]. Anti-CD47 MAbs, but not anti-SIRPα MAbs, also suppressed the growth of L1210 in an *in vivo* sub-cutaneous tumor transplantation assay, using RAG-1-deficient (knockout; KO) mice that lack T cells and B cells as recipients, compared to control MAbs (Fig. 1g and Extended Data Fig. 2e).

In the human system, blocking anti-human CD47 MAbs B6H12 and AO-176, as well as blocking human SIRPα-Fc fusion protein TTI-621 and high-affinity variant ALX148, promoted the capacity of blood-derived human macrophages to phagocytose human lymphoma cell line Raji, compared to control IgG (Fig. 1h and Extended Data Fig. 2f). The augmented phagocytosis of Raji was SLAMF7-dependent (Fig. 1i). However, blocking anti-human SIRPα MAbs KWAR23 and 18D5 did not augment phagocytosis (Fig. 1h). A similar lack of effect of blocking anti-human SIRPα MAbs KWAR23, 18D5, 50A and 40A was seen with mouse BMDMs ectopically expressing human SIRPα as phagocytes (Extended Data Fig. 2f). Many of these human SIRPα-CD47-targeting agents are being tested in the clinic as anti-cancer therapies[3].

Hence, blockade of CD47, but not of SIRPα, promoted *in vitro* phagocytosis and *in vivo* elimination of tumor cells expressing the cell-intrinsic pro-phagocytic ligand SLAMF7.

Genetic deficiency of CD47 or SIRPα phenocopies the impact of pharmacological blockade

To exclude the possibility that the divergent functional consequences of CD47 blockade and SIRPα blockade were due to differences in affinity or other properties of the blocking agents, the impacts of genetic ablation of CD47 on target cells or of SIRPα on macrophages were compared (Fig. 2a). Wild-type BMDMs displayed greater phagocytosis of CD47 KO L1210, CD47 KO activated T cells, and CD47 KO lymphoma cell lines Raji and Daudi, compared to their wild-type CD47-positive counterparts, as described[5] (Fig. 2b–e and Extended Data Fig. 3a). However, compared to wild-type BMDMs, BMDMs from a new SIRPα KO mouse strain generated in a pure C57BL/6 (B6) background did not exhibit augmented phagocytosis of CD47-positive targets (Fig. 2b–e and Extended Data Fig. 3a). Like wild-type BMDMs, SIRPα KO BMDMs displayed greater phagocytosis of target cells only when CD47 was absent from targets. An increase in phagocytosis was also noted when SIRPα KO BMDMs were pre-treated with the pro-inflammatory stimulus lipopolysaccharide (LPS), which enables phagocytosis via a SLAMF7-independent mechanism involving CD18-associated integrins, as reported[15] (Extended Data Fig. 3b,c). Similar results were obtained in *in vivo* elimination assays using L1210, expressing or not expressing CD47, that were injected in mice expressing or not expressing SIRPα (Fig. 2f and Extended Data Fig. 3d).

The lack of impact of SIRPα deficiency on phagocytosis was unlikely to be due to altered development or differentiation of SIRPα KO BMDMs, as suggested by their unchanged RNA sequencing profiles, compared to wild-type BMDMs (Extended Data Fig. 4a). Moreover, other than lack of SIRPα, SIRPα KO BMDMs displayed no alteration in expression of various cell surface markers, including SLAMF7 (Extended Data Fig. 4b). Analogous findings were made with BMDMs from a second newly created SIRPα KO mouse strain (Extended Data Fig. 4c–e). It should be noted that another group reported that a different SIRPα KO mouse strain displayed changes in RNA expression in splenic macrophages, compared to a wild-type mouse[24]. Whereas the basis for the divergence with our results is not known, it may reflect the different source of macrophages, the mixed genetic background (C3H/HeN-C57BL/6) or effects of the microbiome, in the mouse strain studied by the other group.

Thus, loss of CD47 on tumor cells or of SIRPα on macrophages mimicked the distinct consequences of blockade of CD47 or SIRPα on phagocytosis.

Inactivation of CD47 or SIRPα promotes phagocytosis of antibody-opsonized tumor cells

To ascertain if the disparate effects of blockade or loss of CD47 and SIRPα extended to other pro-phagocytic receptors, tumor cells were “opsonized” by antibodies (IgG) or complement ($C3b_i$), which trigger FcRs or CD11b (Mac-1), respectively[8] (Fig. 3a–e). Unlike with non-opsonized targets (Fig. 1,2), anti-SIRPα MAbs were as efficient as anti-CD47 MAbs at augmenting phagocytosis of IgG-opsonized L1210 or Raji, compared to control MAbs (Fig. 3a–c). In an analogous way, SIRPα KO BMDMs displayed greater phagocytosis of IgG-opsonized targets, compared with wild-type BMDMs (Fig. 3d). In addition, mice lacking SIRPα exhibited slower growth of IgG-opsonized CD47-positive L1210 in an *in vivo* tumor assay, compared to mice expressing SIRPα (Fig. 3f and Extended Data Fig. 5). Similar effects were noted with complement-opsonized targets (Fig. 3e).

Therefore, blockade or loss of CD47 on target cells and blockade or loss of SIRPα on macrophages were equally efficient at augmenting phagocytosis of targets opsonized by exogenous ligands targeting FcRs or CD11b.

CD47 physically interacts in *cis* with SLAMF7 on tumor cells

One possibility to explain the inability of blockade or loss of SIRPα to augment phagocytosis of non-opsonized targets was that CD47 triggered inhibitory receptors other than SIRPα that compensated for blockade or loss of SIRPα. However, a soluble CD47-Fc fusion protein displayed no residual binding to SIRPα KO BMDMs, suggesting that this notion was unlikely (Fig. 4a). Because expression of SLAMF7 on targets is critical for phagocytosis during CD47 blockade (Fig. 1f), another scenario was that CD47 was interacting in *cis*, directly or indirectly, with SLAMF7 at the surface of tumor cells, thereby disallowing SLAMF7 on tumor cells from triggering SLAMF7 on macrophages.

To address this idea, CD47 was immunoprecipitated from L1210 tumor cells and potential CD47-associated proteins were detected by mass spectrometry. As the anti-CD47 MAb targets the extracellular domain of CD47, L1210 cells expressing a Flag-tagged variant of CD47 were generated and immunoprecipitation of CD47 was conducted using anti-Flag

MAbs (Extended Data Fig. 6a,b). These cells expressed amounts of Flag-tagged CD47 analogous to those of endogenous CD47 in parental L1210 cells (Extended Data Fig. 6a). CD47 abundantly co-immunoprecipitated with SLAMF7 in these cells (Fig. 4b and Extended Data Fig. 6c). Several other proteins were also detected, although less prominently and none was a known pro-phagocytic ligand. Co-immunoprecipitation of epitope-tagged versions of CD47 and SLAMF7 was also identified in transiently transfected 293T cells (Fig. 4c).

To confirm that CD47 and SLAMF7 were in physical proximity at the plasma membrane, fluorescence resonance energy transfer (FRET) studies were conducted, using CD47 KO 293T cells expressing a CD47 variant labeled with an energy acceptor and a SLAMF7 variant labeled with an energy donor (Fig. 4d,e and Extended Data Fig. 6d). FRET can be detected when two molecules are positioned within 10 nm of each other[25]. It reflects a transfer of fluorescence from the donor to the acceptor. FRET is identified by ascertaining if fluorescence of the donor is augmented when the acceptor is photobleached. We found that photobleaching of acceptor-labeled CD47 resulted in an increase in fluorescence of donor-labeled SLAMF7, indicating energy transfer from SLAMF7 to CD47 (Fig. 4d,e).

The FRET between CD47 and SLAMF7 was reduced by a blocking anti-CD47 MAb, which interacts with the SIRPα-binding domain of CD47, compared to control IgG (Fig. 4d,e). This effect was not due to hindrance with dye labeling by the blocking MAbs (Extended Data Fig. 6e). It was also diminished by a point mutation in the SIRPα-binding domain of CD47 [phenylalanine 37-to-aspartate 37 (F37D) mutation]. Likewise, it was reduced by mutations of the putative self-ligand-binding sequences of SLAMF7 [arginine 75-to-alanine 75 (R75A) or glutamate 77-to-alanine 77 (E77A) mutations][26, 27] (Extended Data Fig. 7a–d).

We also analyzed the proximity of endogenous CD47 and SLAMF7 on L1210 cells, using a proximity ligation assay (PLA)[28, 29]. PLA can detect proximity of two molecules when they are within 40 nm of each other. After fixing the cells to stabilize proximity, cells are incubated with primary antibodies against the two proteins of interest, followed by oligonucleotide-linked secondary antibodies recognizing each of the primary antibodies. Then, proximity is detected by PCR with complementary oligonucleotides coupled to fluorochromes, and fluorescence microscopy. We observed fluorescent dots, presumably representing CD47-SLAMF7 complexes, in parental L1210 cells, but not in L1210 cells lacking CD47 or reconstituted with the F37D CD47 mutant (Fig. 4f,g).

As expected, the F37D CD47 mutant failed to repress phagocytosis when introduced in CD47 KO L1210 and did not bind a SIRPα-Fc fusion protein, compared to wild-type CD47 (Extended Data Fig. 8a,b). Furthermore, the R75A and E77A SLAMF7 mutants failed to rescue the pro-phagocytic effect of SLAMF7 when expressed in SLAMF7 KO T cells, and did not bind to a soluble SLAMF7-Fc fusion protein, compared to wild-type SLAMF7, in keeping with the idea that these mutations abolished the SLAMF7-SLAMF7 homotypic interaction (Extended Data Fig.7b, 8c,d).

Finally, to assess if the physical proximity of CD47 and SLAMF7 was due to a direct interaction, FRET assays were performed using cell-free large unilamellar vesicles (LUVs), as described[30, 31], which were reconstituted with purified extracellular domains of CD47 and SLAMF7 labeled with energy acceptor and donor, respectively (Extended Data Fig. 7e). Addition of CD47, but not of unrelated receptor PD-1, quenched the fluorescence of SLAMF7, indicating energy transfer and proximity (Extended Data Fig. 7f). The FRET was reduced by blocking anti-CD47 MAb or blocking anti-SLAMF7 MAb 4G2 (Extended Data Fig. 7g). Binding of soluble CD47-Fc fusion protein on control or CD47 KO Raji cells was not detectable (Extended Data Fig. 7h). This is probably because the *cis* interaction between CD47 and SLAMF7 is facilitated or stabilized when both are positioned within the cell surface, perhaps in specialized membrane microdomains or structures[32].

Together, these data implied that CD47 interacted in *cis* with SLAMF7 at the surface of tumor cells and that this interaction was mediated by their canonical ligand-binding domains. Experiments with LUVs suggested that this interaction may be direct.

Evidence that freeing of SLAMF7 from CD47 promotes phagocytosis

To evaluate if deliverance of SLAMF7 from CD47 was a trigger for phagocytosis, two approaches were used. First, using a binding assay with a SLAMF7-positive cell line, we observed that blocking anti-CD47 MAbs augmented the ability of a soluble SLAMF7-Fc fusion protein to bind to these cells, compared to a control Fc fusion protein (Fig. 5a,b). No binding was seen when the cell line lacked SLAMF7 (Fig. 5c).

Second, we reasoned that overexpression of SLAMF7 on tumor cells might create a pool of CD47-free SLAMF7 that could elicit phagocytosis. When SLAMF7 was overexpressed (~30-fold) in L1210 cells, there was a recovery of phagocytosis in SIRPα KO macrophages, to nearly the same extent as that seen with CD47 deficiency (Fig. 5d,e). This effect required SLAMF7 on macrophages (Fig. 5f). There was no increase in phagocytosis if tumor cells overexpressed SLAMF7 but lacked CD47 (Fig. 5d,e).

Combined with the results showing that a CD47 mutant (F37D) unable to bind SLAMF7 in *cis* did not suppress phagocytosis by SIRPα KO BMDMs (Extended Data Fig. 8a,b), these data suggested that the release of SLAMF7 from CD47, by blocking anti-CD47 antibodies, enforced expression of SLAMF7 or mutation of CD47, promoted phagocytosis.

Identification of a first-in-class agonistic anti-SLAMF7 MAb

To obtain more direct evidence that freeing SLAMF7 from CD47 triggered phagocytosis, we sought to identify pro-phagocytic anti-SLAMF7 MAbs, which acted by dissociating SLAMF7 from CD47. To this end, we generated a large collection of novel anti-human SLAMF7 MAbs. We also analyzed elotuzumab, which is a non-blocking anti-SLAMF7 MAb used in the clinic for the treatment of multiple myeloma[33] (Fig. 6a). All MAbs reacted with human SLAMF7, but not with mouse SLAMF7, and were modified to be Fc-silent (see Methods).

One newly generated MAb, MAb Z10, was able to stimulate phagocytosis of human target Raji (Fig. 6a,b). This effect was seen with SIRPα KO mouse BMDMs, but not with wild-

type BMDMs, because mouse SIRPα can bind to human CD47 and mouse SLAMF7 can bind to human SLAMF7[5, 15]. The combined impact of MAb Z10 and inactivation of SIRPα was analogous to that of anti-CD47 MAb B6H12. None of the other anti-SLAMF7 MAbs, including elotuzumab, had a pro-phagocytic impact. MAb Z10 also triggered phagocytosis of human SLAMF7-positive Daudi and multiple myeloma cell line MM.1S, and of activated mouse T cells rendered positive for human SLAMF7 by transgenesis (Extended Data Fig. 9a,b).

The agonistic effect of MAb Z10 was also seen with human macrophages, and with mouse macrophages retrovirally transduced by human SLAMF7, in the presence of Raji as targets (Fig. 6c–e). However, no impact was seen when macrophages expressed human SLAMF7, but targets expressed mouse SLAMF7 (Fig. 6f), indicating that the pro-phagocytic effect of MAb Z10 required human SLAMF7 on the target cells (Extended Data Fig. 9c).

In an *in vivo* sub-cutaneous tumor growth assay using RAG-1 KO mice and Raji human tumor cells, the combination of anti-SIRPα MAb #27 plus anti-SLAMF7 MAb Z10 was better than anti-CD47 B6H12 at suppressing tumor growth and at increasing survival, compared to control IgG (Fig. 6g,h and Extended Data Fig. 9d). No anti-tumor effect was seen with anti-SIRPα MAb #27 alone, anti-SLAMF7 MAb Z10 alone, anti-SIRPα MAb #27 plus anti-SLAMF7 elotuzumab, or anti-SLAMF7 elotuzumab alone.

Thus, anti-SLAMF7 MAb Z10 was an agonistic MAb that stimulated phagocytosis and prevented tumor growth, when combined with SIRPα blockade. The combination was apparently more effective than a blocking anti-CD47 MAb. No similar effect was seen with anti-SLAMF7 elotuzumab. The impact of MAb Z10 required binding to SLAMF7 on tumor cells, not on macrophages.

Anti-SLAMF7 MAb Z10 frees SLAMF7 from CD47

Using FRET assays, we noted that MAb Z10, but not elotuzumab, dissociated the *cis* interaction between CD47 and SLAMF7, in a manner analogous to anti-CD47 MAb B6H12 (Fig. 7a,b). Co-immunoprecipitation of CD47 and SLAMF7 in 293T cells was also disrupted by MAb Z10 (Extended Data Fig. 10a). Furthermore, in confocal microscopy analyses, the combination of MAb Z10 and SIRPα blockade enhanced actin polarization in macrophages exposed to tumor cells, without promoting conjugate formation between macrophages and tumor cells, in a manner comparable to CD47 blockade[5] (Fig. 7c and Extended Data Fig. 10b,c).

To examine if MAb Z10 was targeting the sequences directly involved in SLAMF7-SLAMF7 or, as similar sequences seemed implicated, CD47-SLAMF7 interactions, we first analyzed its binding to chimeras between human and mouse SLAMF7. Like elotuzumab, MAb Z10 interacted with the SLAMF7 second Ig-like domain [Ig(C)], which is not directly involved in the homotypic interaction (Fig. 7d). In contrast, another anti-SLAMF7 MAb, MAb Z8, interacted with the first Ig-like domain [Ig(V)], which is needed for the homotypic interaction (Fig. 7d). Next, we examined if MAb Z10 was able to suppress SLAMF7-dependent phagocytosis. MAb Z10 did not interfere with phagocytosis of CD47 KO Raji or Daudi, which are phagocytosed via SLAMF7, in keeping with the idea that MAb

Z10 was not directly targeting the sequences involved in the SLAMF7-SLAMF7 interaction (Extended Data Fig. 11a,b).

By creating additional chimeras between human and mouse SLAMF7, we found that replacement of amino-acids 169–176 or 181–188 in human SLAMF7 abolished binding of MAb Z10 and elotuzumab, but not of MAb Z8 (Extended Data Fig. 12a). Furthermore, point mutations (to alanines) of human SLAMF7 showed that arginine 181 (R181), asparagine 182 (N182), phenylalanine 183 (F183) or, to a lesser extent, valine 174 (V174) were needed for binding of MAb Z10 and elotuzumab, but not of MAb Z8 (Fig. 7e and Extended Data Fig. 12b). V174 and N182 were more critical for binding of MAb Z10, compared to elotuzumab. The latter finding suggested differences in the binding mechanisms of MAb Z10 and elotuzumab to SLAMF7. Mutation of amino-acids 172, 173 or 177 abolished or greatly reduced binding of all MAbs, implying that these mutations compromised expression of SLAMF7 at the cell surface (Extended Data Fig. 12b).

Hence, like anti-CD47 MAbs, the first-in-class agonistic anti-SLAMF7 MAb Z10 dissociated the CD47-SLAMF7 *cis* interaction on tumor cells. MAb Z10 was not binding the sequences directly involved in the SLAMF7-SLAMF7 interaction. Considering that the same sequences seemed implicated in the CD47-SLAMF7 interaction, it is likely that the effect of MAb Z10 was not due to pure blocking, but perhaps to conformational modification of SLAMF7 leading to dissociation from CD47.

Discussion

In this report, we have identified a previously unknown mechanism by which CD47 prevents phagocytosis. In addition to its ability to trigger the inhibitory receptor SIRPα on macrophages, CD47 physically interacted in *cis* with the pro-phagocytic ligand SLAMF7 on tumor cells, thereby masking the ability of this ligand to engage its receptor on macrophages and to trigger phagocytosis (Extended Data Fig. 13a). Relief of both mechanisms was needed to enable phagocytosis of tumor cells, unless the SIRPα-independent mechanism was bypassed by decorating the tumor cells with exogenous antibodies or complement, or by providing inflammatory stimuli (Extended Data Fig. 13b).

We postulate that the high efficiency of CD47 at suppressing the function of SLAMF7 was because CD47 is much more abundant than SLAMF7 on target cells. Hence, it easily saturates all ligand-binding surfaces on SLAMF7. This notion was consistent with our overexpression studies of SLAMF7 in L1210 cells (Fig. 5d,e). It was also supported by previously reported quantitative proteomic analyses, whereby CD47 molecules were estimated to be ~10-times more abundant than SLAMF7 molecules in activated T cells[34].

The only known pro-phagocytic ligand co-immunoprecipitating with CD47 in L1210 cells was SLAMF7. Nevertheless, it is possible that CD47 also interacts *in cis* with yet unidentified pro-phagocytic ligands on other cell types. For instance, CD47 may associate with ligands on red blood cells and platelets, which are depleted during CD47 blockade but do not express SLAMF7[3, 7, 18–20]. Although removal of these cell types may be mediated via engagement of FcRs by the Fc portion of anti-CD47 MAbs or SIRPα-Fc fusion proteins,

it is also plausible that CD47 blockade unmasks pro-phagocytic ligands on red blood cells or platelets. Future studies addressing these possibilities are warranted, as they may help design strategies to attenuate the toxicities of SIRPα-CD47 blockade.

The *cis* interaction between CD47 and SLAMF7 involved their canonical ligand-binding domains, which are also implicated in the *trans* interactions with SIRPα or SLAMF7, respectively. Accordingly, the CD47-SLAMF7 association was relieved by blocking anti-CD47 MAbs or SIRPα-Fc fusion proteins, but not by blocking anti-SIRPα MAbs (Extended Data Fig. 13a). Interestingly, it was also alleviated by a first-in-class anti-SLAMF7 MAb, MAb Z10, which potentially acted by conformational modification of SLAMF7 leading to dissociation of SLAMF7 from CD47 (Extended Data Fig. 13a). Given that both CD47 and SLAMF7 are members of the Ig superfamily, which encompasses several proteins capable of direct heterotypic interactions, and given the results of our PLA and LUV assays, we postulate that the association between these two molecules may be direct. However, formal demonstration of this notion will require structural analyses of the CD47-SLAMF7 complexes.

Although MAb Z10 had no appreciable single agent anti-tumor activity, it enabled tumor cell elimination *in vitro* and *in vivo* when combined with SIRPα blockade, suggesting an effective new combination therapy against SLAMF7-positive malignancies such as multiple myeloma and lymphoma. This effect was not observed with elotuzumab. Interestingly, in our *in vivo* model with Raji cells, MAb Z10 plus SIRPα blockade was more effective than CD47 blockade at suppressing tumor growth. Although this difference remains to be confirmed using other tumor models and in the clinic, one possibility is that the higher levels of CD47 on tumor cells, coupled to the large “sink” of broadly distributed CD47 on normal cells in humans, may make CD47 more difficult than SIRPα and SLAMF7 to saturate with antibodies. For the same reasons, SIRPα blockade may be preferable over CD47 blockade when used in combination with tumor opsonizing MAbs such as rituximab to trigger ADCP (Fig. 3). Another advantage of MAb Z10 plus SIRPα blockade over CD47 blockade may be that hematological cell types depleted during CD47 blockade but seemingly spared during SIRPα blockade, such as red blood cells and platelets, do not express SLAMF7[3, 7, 18–20]. Hence, these cells may be spared during MAb Z10 plus SIRPα blockade. However, this may not be the case for activated T cells, which express SLAMF7. Future studies will be needed to address these ideas.

In addition to enhancing our comprehension of how CD47 prevents phagocytosis and to providing insights into the relative advantages of targeting SIRPα versus CD47 for therapeutic purposes, these results exemplified the notion that blockade of receptors and blockade of their ligands for therapy do not always have the same impact. This dichotomy can translate into differences in efficacy and toxicity. This phenomenon occurs because receptors and their ligands can have numerous and at times divergent mechanisms of action. Clearly, a better knowledge of how receptors and their ligands work at the molecular level is crucial for making the best decisions regarding which ones should be targeted in therapies of human diseases.

Methods

Mice

Mice lacking SIRPα (*Sirpa*$^{-/-}$) were generated in our laboratory using fertilized C57BL/6J oocytes and CRISPR-Cas-based genomic editing. The following guide RNAs were used: 5′- AGCAGCGGCCCTAGGCGGCC-3′, 5′-GCCCGGCCCCTGGCCGCCTA-3′ and 5′-TCCGCGTCCTGTTTCTGTAC-3′. After birth, mice were screened by flow cytometry and sequencing of the *Sirpa* gene. Strains bearing a 593-nucleotide (#46) or 11-nucleotide (#54) deletion in exon 2 of *Sirpa* were chosen. These deletions resulted in a frameshift in the second coding exon of the *Sirpa* gene and caused loss of SIRPα expression by flow cytometry. Heterozygous knock-out (KO) mice were backcrossed to the C57BL/6J background for more than 10 generations and subsequently bred to homozygosity for experimentation. The #46 mouse strain was used for most experiments, unless specified. Mice lacking all SFRs (SFR KO) or SLAMF7 (*Slamf7*$^{-/-}$), and mice expressing a human (h) *SLAMF7* bacterial artificial chromosome transgene (hSLAMF7 BAC Tg mice), in the C57BL/6J background, were described elsewhere[5, 35]. CD47 KO (*Cd47*$^{-/-}$), RAG-1 KO (*Rag1*$^{-/-}$) and C57BL/6J mice were obtained from the Jackson Laboratory. SIRPα KO mice were bred with SFR KO or SLAMF7 KO mice to create SIRPα-SFR double (D) KO mice and SIRPα-SLAMF7 DKO mice. hSLAMF7 BAC Tg mice were bred with SLAMF7 KO mice to create SLAMF7 KO-hSLAMF7 BAC Tg mice. RAG-1-SIRPα DKO mice were generated in the same manner as SIRPα KO mice, except that RAG-1 KO oocytes were used for micro-injection of guide RNAs. This approach was needed because the *Sirpa* and *Rag1* genes are located on the same chromosome. A mouse strain bearing a 168-nucleotide deletion in exon 2 of *Sirpa* was chosen. This deletion resulted in a frameshift in the second coding exon of the *Sirpa* gene and caused loss of SIRPα expression by flow cytometry.

All mice were maintained in the C57BL/6J background. They were kept in a specific pathogen-free environment. Either males or females were used, between 8 to 12 weeks of age. Littermates were used as control in most experiments, except for some studies where wild-type syngeneic, age and sex-matched mice were used. Animal experimentation was done in accordance to the Canadian Council of Animal Care and approved by the IRCM Animal Care Committee.

Cells

Macrophages were generated as described[5]. Briefly, for mouse macrophages, bone-marrow-derived macrophages (BMDMs) were generated by growing freshly isolated bone marrow cells for 7 days in medium supplemented with 30% (vol/vol) L929 cell-conditioned medium, as a source of colony-stimulating factor-1 (CSF-1). Human macrophages were produced from peripheral blood mononuclear cells, which were isolated from healthy donors using Ficoll-Paque PLUS (Cat# 36–101-6383, GE Healthcare), according to the manufacturer's protocol and as approved by the IRCM Human Ethics Board. Peripheral blood mononuclear cells were then seeded onto Petri dishes containing serum-free RPMI medium for 30 min. After gentle washes to remove non-adherent cells, adherent cells (which mostly represent monocytes) were differentiated into macrophages by culture in medium supplemented with 10% human serum and 10 ng ml^{-1} CSF-1 (Cat# 300–25, Peprotech) for 7 days.

Mouse $CD4^+$ or $CD8^+$ T cells, depleted of natural killer T (NKT) cells using anti-NK1.1 monoclonal antibody (MAb), were purified from spleen by negative selection using the EasySep Purification Kits (Cat# 19852 or 19853, STEMCELL Technologies). Activated $CD4^+$ T cells were obtained by stimulating $CD4^+$ T cells with 4 μg ml^{-1} concanavalin A (Cat# C5275, Sigma-Aldrich) for 2 days, followed by expansion for 3 days in medium containing 50 units ml^{-1} interleukin-2 (Cat# 212–12, Peprotech). Activated $CD8^+$ T cells were obtained by stimulating $CD8^+$ T cells with 3 μg ml^{-1} Fc-silent anti-CD3 (145–2C11, Absolute Biotech Company) plus 1 μg ml^{-1} Fc-silent anti-CD28 (D665, Absolute Biotech Company) MAbs for 2 days.

L1210 (CCL-219), P815 (TIB-64), SP2/0 (CRL-1581), Raji (CCL-86), Daudi (CCL-213), MM.1S (CRL-2974), L929 (CCL-1), EL-4 (TIB-39), FO (CRL-1646), 293T (CRL-3216) and Phoenix-Eco (CRL-3214) were obtained from American Type Culture Collection. The T cell hybridoma line BI-141 was reported elsewhere[36]. Immune cells were authenticated by the provider and verified by flow cytometry. All cells were negative for Mycoplasma.

CRISPR-Cas9 knockout and retroviral infection

CD47 KO L1210 cells and CD47 KO 293T cells were generated by CRISPR-Cas-mediated genome editing, using plasmid PX458 (Cat# 48138, Addgene) and the following guide RNAs: mouse CD47 (mCD47): 5′-CACCGAGCAACAGCGCCGCCGCCAA-3′ and 5′-CACCGTTGGCGGCGGCGCTGTTGCT-3′; human CD47 (hCD47): 5′-CTGGTAGCGGCGCTGTTGCT-3′. CD47 KO Raji cells and CD47 KO Daudi cells were generated using the Neon Transfection System Kit (Cat# MPK10096, Thermo Fisher Scientific), guide RNA 5′-CTACTGAAGTATACGTAAAG-3′ or scrambled guide RNA (Cat# 1072544, IDT), and the Cas9 nuclease (Cat# 1081058, IDT). CD47 KO cells were then purified by cell sorting.

Constructs encoding wild-type mouse (m) CD47, Flag-tagged mCD47 (Flag tag added at the carboxyl terminus), phenylalanine 37-to-aspartate 37 (F37D) mCD47, wild-type mSLAMF7, arginine 75-to-alanine 75 (R75A) mSLAMF7, glutamate 77-to-alanine 77 (E77A) mSLAMF7, wild-type mSIRPα, mSIRPα first Ig-like (variable; V) domain, wild-type hCD47, hSIRPα version 1 (V1) and hSIRPα V2 were generated by PCR or overlap extension PCR. They were then cloned into either the pFB-GFP or the pMIGR-GFP retroviral vector (which used the mouse stem cell virus promoter), which also encode the green fluorescent protein (GFP). For L1210 derivatives overexpressing SLAMF7, SLAMF7 was cloned into a promoter-modified pFB-GFP (which used the EF-1α promoter). After transfection in Phoenix-Eco cells, viral supernatants were recovered and used for spin infection of the indicated cell lines or primary cells. Plasmids expressing GFP alone were used as controls. 48 hours after retroviral infection, GFP-positive cells were sorted, expanded and used for experimentation. L1210, EL-4 and BI-141 were sorted twice. L1210 derivatives expressing the Tac antigen (hCD25) were generated as described[5].

Recombinant proteins

To produce Fc fusion proteins containing the extracellular domain of mCD47, mSLAMF7, mSIRPα, mSIRPβ1a, mSIRPβ1b, mSIRPβ1c, hCD47, hSLAMF7, hSLAMF7 first Ig-

like [variable; Ig(V)] domain fused to mSLAMF7 second Ig-like [constant; Ig(C)] domain, or mSLAMF7 Ig(V) fused to hSLAMF7 Ig(C), cDNAs were cloned into pFc-hIgG1(LALAPG), which encodes in frame the Fc portion of human IgG1 (hIgG1) with the "LALAPG" mutation (leucine 234-to-alanine 234; leucine 235-to-alanine 235; proline 329-to-glycine 329) that prevents binding to Fc receptors (FcRs). SIRPα-Fc fusion proteins TTI-621[12] and its high-affinity variant ALX148[13] were produced by synthesizing the cDNAs from published sequences, followed by cloning into pFc-hIgG1(LALAPG). For production, cDNAs were transfected in 293T cells. Then, fusion proteins were purified with protein A Sepharose (Cat# GE17–1279-03, Sigma-Aldrich). All recombinant proteins were quantified by SDS-PAGE and Coomassie blue staining, using bovine serum albumin (BSA) as standard.

To produce recombinant versions of mCD47, mSLAMF7, hPD-1 and hPD-L1, cDNAs encoding their extracellular segment, in which a SNAP tag was inserted after the amino-terminal signal peptide and a 10x histidine (His) tag was inserted after the carboxyl terminus of the extracellular domain, were cloned in pPPI4 vector. After transfection in 293T cells, recombinant proteins were purified from cell culture medium using GE Ni Sepharose® Excel (GE17371201, Sigma-Aldrich) and eluted with 0.5 M imidazole. Proteins were further purified by size exclusion, using a Superdex 200 Increase 10/300 GL column (Cat# GE28990944, Sigma-Aldrich), in 4-(2-hydroxyethyl)-1-piperazineethanesulfonic acid (HEPES)-buffered saline buffer (50 mM HEPES-NaOH, pH 7.5, 150 mM NaCl, 10% glycerol). Gel-filtered proteins were labeled either with SNAP-Cell-505 (Cat# S9103S, New England Biolabs) or with SNAP-Cell-TMR (Cat# S9105S, New England Biolabs) following the manufacturer's instructions. Free dye was removed using a PD-10 desalting column (Cat# 87766, Thermo Fisher Scientific). All proteins were quantified by SDS-PAGE and Coomassie blue staining, using BSA as a standard.

Monoclonal antibodies

To generate anti-mSIRPα MAbs, SIRPα KO mice were immunized with recombinant mSIRPα-Fc fusion proteins. Splenocytes from hyperimmune mice were then fused with FO cells using polyethylene glycol (Cat# P7306, Sigma-Aldrich), and cultured in hypoxanthine-aminopterin-thymidine medium for ~8 days. Hybridomas were initially screened by ELISA using the mSIRPα-Fc fusion protein or an irrelevant Fc fusion protein as control. The hybridomas producing anti-mSIRPα antibodies were then subjected to two rounds of sub-cloning. Anti-mSIRPα MAbs were screened for: 1) the capacity to stain EL-4 cells expressing full-length mSIRPα or a variant of mSIRPα containing only the first Ig-like domain, which is implicated in CD47 binding, using flow cytometry; 2) the ability to block the binding of a mCD47-Fc fusion protein to EL-4 cells expressing mSIRPα, using flow cytometry; 3) the ability to bind SIRPα-Fc, but not SIRPβ-Fc fusion proteins, using ELISA. Anti-mSIRPα MAbs #23 and #27 exhibited blocking activity towards SIRPα and did not cross-react with any of the SIRPβ isoforms.

Anti-hSLAMF7 hybridomas were generated in the similar way, except that SLAMF7 KO mice and recombinant hSLAMF7-Fc fusion proteins were utilized. After two rounds of sub-cloning, anti-hSLAMF7 MAbs were screened for: 1) the ability to bind hSLAMF7-Fc, but

not mSLAMF7-Fc. They were also tested for binding to hSLAMF7(V)-mSLAMF7(C)-Fc or mSLAMF7(V)-hSLAMF7(C)-Fc, to determine if they reacted with the first or second Ig-like domain of hSLAMF7; 2) the capacity to stain EL-4 cells expressing or not hSLAMF7, or CD47 KO 293T cells expressing or not hSLAMF7, or the human-mouse SLAMF7 chimeras; 3) the capacity to block the phagocytosis of CD47 KO Raji or CD47 KO Daudi by wild-type BMDMs. Anti-hSLAMF7 MAbs Z1, Z8, Z9 and Z27 bound specifically to the first IgG-like domain, whereas MAbs Z10, Z26, Z30, Z46 and elotuzumab (Elo) bound specifically to second Ig-like domain. MAb Z8 was a blocking MAbs. MAbs Z10 and elotuzumab were non-blocking MAbs.

Blocking anti-mSLAMF7 MAb 4G2 was generated in our laboratory[16]; blocking anti-mCD47 hybridoma Miap301 was provided by Dr. Timo van den Berg (Sanqin Institute, Amsterdam, The Netherlands); blocking anti-mSIRPα hybridoma MY-1 was provided by Takashi Matozaki (Kobe University, Kobe, Japan); and blocking anti-hSLAMF7 hybridoma 162 was reported elsewhere[37].

To create recombinant versions of blocking anti-mSIRPα MAb MY-1, blocking anti-mSIRPα MAbs #23 and #27, blocking anti-mCD47 MAb Miap301, blocking anti-mSLAMF7 MAb 4G2, blocking anti-hSLAMF7 MAb 162, and novel anti-hSLAMF7 MAbs Z1, Z8, Z9, Z10, Z26, Z27, Z30 and Z46, cDNA sequences encoding the variable regions of heavy chain (VH) and light chain (VL) were determined using total cellular RNA from the hybridomas, followed by RNA sequencing or reverse transcription-PCR, as described[38]. To create recombinant versions of control immunoglobulin G (IgG) MAb MOPC21, blocking anti-hSIRPα MAbs KWAR23, 18D5, 50A and 40A, blocking anti-hCD47 MAbs B6H12 and AO-176, and non-blocking anti-hSLAMF7 MAb elotuzumab, VH and VL sequences were obtained from previous studies[14] or patents (WO2017178653A2, US10851164B2, US20200095318, US7709610B2, EP2569013A2). cDNAs encoding these sequences were then synthesized commercially. In all cases, the VH- and VL-encoding cDNAs were cloned in frame into one or both of the following expression plasmids[38]: pAb-mIgG2a(LALAPG), which contains genes encoding Fc-silent mouse IgG2a (mIgG2a) with the LALAPG mutation, and pAb-mIgK; pAb-hIgG1(LALAPG), which contains genes encoding Fc-silent hIgG1 with the LALAPG mutation, and pAb-hIgK. Recombinant MAbs were then expressed in 293T cells and purified with protein A Sepharose (Cat# GE17–1279-03, Sigma-Aldrich). All recombinant MAbs were quantified by SDS-PAGE and Coomassie blue staining, using BSA as a standard.

For opsonization of target cells with IgG, Fc-intact anti-hCD25 MAb 7G7 (mIgG2a; BioXCell) and Fc-intact anti-hCD20 MAb S18015E (mIgG2a; BioLegend) were used. For flow cytometry assays, we used anti-CD45 MAb 30-F11, anti-CD11b MAb M1/70, anti-F4/80 MAb BM8, anti-Ly6G MAb 1A8, anti-NK1.1 MAb PK136, anti-SIRPα MAb P84, anti-CD64 VX54–5/7.1, anti-CD16/32 MAb 93, anti-CD18 MAb M18/2, anti-CD11a MAb M17/4, anti-CD11c MAb N418, anti-CD200R1 MAb OX-110, anti-Flag MAb L5, and anti-rat IgG Poly4054. All were obtained from Biolegend. For immunoprecipitations and immunoblots, we utilized anti-Flag MAb M2 (Sigma-Aldrich), anti-Myc MAb 9B11 (Cell Signaling Technology), anti-mCD47 MAb AF1866 (R&D Systems), anti-mSLAMF7 rabbit antiserum (generated in our laboratory), anti-hCD47 MAb D3O7P (Cell Signaling

Technology) and anti-hSLAMF7 E5C4M (Cell Signaling Technology). Anti-β-actin AC-74 (Sigma-Aldrich) was used for immunofluorescence.

Phagocytosis assays

Phagocytosis was evaluated using a microscopy-based assay or a pHrodo-based assay, as described[15]. For the microscopy-based assay, 5×10^4 macrophages were seeded in a 24-well tissue culture plate. The next day, target cells were labeled with 2.5 μM of carboxyfluorescein succinimidyl ester (CFSE, Cat# C34554, Life Technologies). After incubating macrophages in serum-free medium for 1 hour, 2×10^5 CFSE-labeled target cells were added to macrophages for 2 hours, in the presence or absence of 10 μg ml^{-1} Fc-silent MAbs. Macrophages were then washed and imaged with an inverted microscope (Carl Zeiss Axiovert S100 TV). In each experiment, 5 images per condition were randomly chosen. There were about 60 to 100 macrophages in each image. The phagocytosis efficiency was calculated as the number of macrophages containing $CFSE^+$ target cells per 100 macrophages. For Extended Data Fig. 2c,d, macrophages or L1210 cells were pre-treated with anti-SIRPα MAb or anti-CD47 MAb, respectively. Cells were then extensively washed to remove unbound antibodies before the phagocytosis assay. For Extended Data Fig. 3b,c, macrophages were pre-treated with the pro-inflammatory stimulus lipopolysaccharide (LPS, Cat# L4516, Sigma-Aldrich) before the phagocytosis assay. For the pHrodo-based assay, target cells were pre-labeled with 100 ng ml^{-1} of pHrodo™ green STP ester (Cat# P35369, Thermo Fisher Scientific), prior to addition to macrophages. pHrodo dyes are non-fluorescent at neutral pH and become fluorescent in acidic environments such as phagolysosomes. After 2 hours, cells were harvested and stained with anti-F4/80 MAb BM8 (Biolegend) to identify macrophages and analyzed by flow cytometry. For phagocytosis of IgG-coated tumor cells, L1210 expressing Tac (hCD25) were opsonized with anti-hCD25 MAb 7G7 (mIgG2a) for 30 min, prior to the phagocytosis assays. Conversely, Raji were opsonized with anti-hCD20 MAb S18015E (mIgG2a). For phagocytosis of $C3b_i$-opsonized tumor cells, L1210 was incubated with C5-deficient serum (Cat# C1163, Sigma-Aldrich) for 30 min, prior to the phagocytosis assay.

Soluble Fc fusion protein binding assay and flow cytometry

To test binding of the mCD47-Fc fusion protein to cells, BMDMs were detached from plates by treatment with phosphate-buffered saline (PBS) containing 2 mM ethylenediaminetetraacetic acid and washed. After blocking Fc-receptors with a mix of mIgG2a MAb 7G7 and anti-CD16/32 MAb 2.4G2, cells were incubated for 30 min on ice with mCD47-Fc (hIgG1) (Cat# 1866-CD-050, R&D Systems) or mCD47-Fc (hIgG1 LALAPG) (produced in our laboratory). After the incubation period, cells were washed again and incubated for 30 min on ice with Alexa Fluor 647-labeled $F(ab')_2$ fragments goat anti-human IgG1, Fc-specific (Cat# 109–606-098, Jackson Immune Research). After additional washes, fluorescence was evaluated by flow cytometry. To examine binding of the mSLAMF7-Fc fusion protein to cells, BI-141 cells expressing or not expressing mSLAMF7 were incubated for 30 min on ice with 10 μg ml^{-1} anti-mCD47 MAb (mIgG2a LALAPG). Subsequently, cells were stained with various concentrations of mSLAMF7-Fc (hIgG1 LALAPG) plus Alexa Fluor 647-labeled $F(ab')_2$ fragments goat anti-human IgG1, Fc-specific (Cat# 109–606-098, Jackson Immune Research) for 5 min on ice. After additional

washes, fluorescence was evaluated by flow cytometry. To determine the impact of SLAMF7 mutations on homotypic binding to SLAMF7, BI-141 cells expressing wild-type SLAMF7 or mutated mSLAMF7 (R75A or E77A) were incubated with mSLAMF7-Fc (hIgG1 LALAPG) on ice for 30 min, followed by flow cytometry. To ascertain the effect of CD47 mutations on binding to SIRPα, CD47 KO 293T cells and CD47 KO L1210 cells expressing wild-type mCD47 or mutated mCD47 (F37D) were incubated with mSIRPα-Fc (hIgG1 LALAPG) on ice for 30 min. Cells were then washed and incubated with Alexa Fluor 647-labeled $Fab')_2$ fragments goat anti-human IgG1, Fc-specific (Cat# 109–606-098, Jackson Immune Research) on ice for 30 min. After additional washes, fluorescence was evaluated by flow cytometry. To detect binding of the hCD47-Fc fusion protein to control or CD47 KO Raji cells, cells were incubated for 30 min on ice with hCD47-Fc (hIgG1 LALAPG). Subsequently, cells were stained with Alexa Fluor 647-labeled $F(ab')_2$ fragments goat anti-human IgG1, Fc-specific (Cat# 109–606-098, Jackson Immune Research) for 30 min on ice, followed by flow cytometry. To address the FcR-binding capacity of Fc-silent and Fc-intact MAbs, wild-type BMDMs, which express a wide range of FcRs, were incubated with or without Fc-intact (mIgG2a) or Fc-silent (mIgG2a LALAPG) IgG MOPC21, or Fc-intact (hIgG1) or Fc-silent (hIgG1 LALAPG) anti-hSLAMF7 MAb Z10, prior to flow cytometry. To test whether anti-CD47 or anti-SLAMF7 MAbs hindered dye labeling, CD47 KO 293T cells, transfected with tagged versions of CD47 or SLAMF7, were stained with Dye 547 or Dye 647 in the presence of control IgG, anti-CD47 MAbs or anti-SLAMF7 MAbs before the flow cytometry assay. To map the binding site of anti-SLAMF7 MAbs on hSLAMF7, CD47 KO 293 T cells were transfected with the indicated hSLAMF7 plasmids for 48 hours, before staining with anti-hSLAMF7 MAbs Z10, Z8 or elotuzumab. To determine expression of cell surface markers, Fc receptors were blocked as above, prior to staining with the indicated antibodies.

Sub-cutaneous tumor transplantation assay

L1210 (0.5×10^6), L1210 derivatives (0.5×10^6) or Raji (5×10^6) were injected sub-cutaneously into the right flank of 8- to 10-week-old RAG-1 KO or RAG-1-SIRPα DKO mice. When the tumor was about 5×5 mm in diameter, mice were injected intraperitoneally with 200 μg of Fc-silent control IgG MAb MOPC21, anti-CD47 MAb Miap301, anti-SIRPα MAb #27, anti-SLAMF7 MAb Z10, anti-SLAMF7 MAb elotuzumab or anti-CD47 MAb B6H12, generated in our laboratory, or Fc-intact anti-hCD25 MAb 7G7 and control IgG MAb C1.18.4 (BioXCell). Experiments were terminated when or before tumor volume reached 1.5 cm^3. For survival assays, mice were euthanized when tumors reached 1.5 cm^3. Tumors were then dissected and weighed. Volumes were also assessed. Tumors were sliced into small pieces and digested with 10 μg ml^{-1} deoxyribonuclease I (Cat# D4513, Sigma-Aldrich) and 25 μg ml^{-1} liberase (Cat# 5401054001, Sigma-Aldrich). Then, cells were passed through a strainer using the plunger end of a syringe. After washing, total cell numbers were determined. Immune cells were detected by staining with the relevant antibodies and flow cytometry.

Conjugate formation and actin polarization assays

Conjugate formation and actin polarization were tested as described[5]. In brief, for the microscopy-based conjugate formation assay, BMDMs were labeled with CTV and plated

overnight. The next day, target cells were labeled with CFSE. Macrophages and target cells were then mixed at a 1:4 ratio in serum-free culture medium in the presence of Fc-silent MAbs, and incubated for 20 min at 37°C to allow conjugate formation. Cells were subsequently washed extensively to remove unconjugated cells. Images were obtained by using a LSM710 confocal microscope (Carl Zeiss). Conjugates between BMDMs and target cells were counted. For the flow cytometry-based conjugate formation assay, macrophages were labeled on ice with anti-F4/80 MAb BM8 (Biolegend), while target cells were labeled with CFSE. After washing, macrophages and targets were mixed with Fc-silent MAbs for various periods of time at 37°C. Conjugates were detected by flow cytometry. To study actin polarization, BMDMs were stained with CTV and seeded onto a confocal tissue dish overnight. The next day, target cells were stained with CFSE. Macrophages and targets were then mixed at a 1:4 ratio in serum-free culture medium with Fc-silent MAbs for 20 min at 37°C. Cells were subsequently fixed, washed and permeabilized, and non-specific staining was blocked in PBS supplemented with 5% BSA for 30 min. Then, cells were washed and incubated for 1 hour with anti-actin MAb AC-74 (Sigma-Aldrich). After washing, cells were incubated for 1 hour with Alexa Fluor 647-conjugated anti-mouse IgG (Cat# 115–605-071, Jackson Immune Research). Cells were then processed and analysed using a LSM710 confocal microscope (Carl Zeiss). Conjugates with full polarization of actin at the area of contact between the macrophage and the target cell were quantitated.

Immunoprecipitations, immunoblots and mass spectrometry

CD47 KO 293T cells were transiently transfected with plasmids encoding mSLAMF7-Myc, mCD47-Flag or both, or control plasmids, using polyethylenimine (PEI, Cat# 23966, Polysciences). The Myc and Flag tags were located at the carboxyl terminus of the proteins. Immunoprecipitation and immunoblot assays were performed as previously described[39]. To test dissociation of CD47-SLAMF7 interactions by MAbs, transfected cells were pre-incubated for 30 min with the indicated MAbs. CD47 KO L1210 cells expressing mCD47-Flag and a Brij99-containing lysis buffer were used for mass spectrometry, as reported elsewhere[5]. The following criteria were used to select potentially relevant CD47 interactors: 1) presence in Flag immunoprecipitates from CD47 KO L1210 cells expressing CD47-Flag, but not from CD47 KO L1210 cells lacking CD47-Flag; 2) observation in a minimum of two of three independent experiments.

RNA sequencing

RNA sequencing was performed as described[40]. In essence, RNA was isolated from wild-type and SIRPα KO BMDMs using the RNeasy Plus Mini Kit (Cat# 74134, Qiagen), according to the manufacturer's instructions. cDNA libraries were prepared using the Illumina TruSeq Stranded mRNA Kit, according to the manufacturer's instructions, and sequenced with the Illumina HiSeq 2000 Sequencer. Read quality was confirmed using FastQC v0.11.8, before alignment using STAR v2.5.0 for the mouse GRCm38 v98 Reference genome. Differential expression analysis was performed with DESeq2 v1.22.2 from the raw alignment counts calculated with FeatureCounts v1.5. Differentially expressed genes were defined as genes with an adjusted p value of <0.05 and $\log_2$ fold change of ≥ 1.0.

PLA assay

Proximity ligation assay (PLA) was performed with a commercial kit according to the manufacturer's recommendation (Cat# DUO92008, Duolink In Situ, Sigma-Aldrich). Briefly, after fixing the cells to stabilize proximity, cells were incubated with Fc-silent human IgG1 anti-SLAMF7 MAb and Fc-silent mouse IgG2a anti-CD47 MAb, followed by oligonucleotide-linked secondary antibodies specifically recognizing each of the primary antibodies. Then, proximity was detected by PCR with complementary oligonucleotides coupled to fluorochromes, and a LSM710 confocal microscope (Carl Zeiss). In each experiment, 5 images per condition were randomly chosen. 100 cells from 3 independent experiments were randomly chosen for quantification.

FRET assay

For the fluorescence resonance energy transfer (FRET) assay, constructs encoding SNAP-tagged wild-type mCD47, mutant mCD47 (F37D) or wild-type hCD47 were co-transfected with constructs encoding CLIP-tagged wild-type mSLAMF7, mSLAMF7 mutants (R75A or E77A) or wild-type hSLAMF7, into CD47 KO 293T cells. After 2 days, cells were collected and seeded onto poly-D-lysine (Cat# P6407, Sigma-Aldrich)-treated confocal microscopy plates. The next day, cells were labeled with SNAP-Surface Alexa Fluor 647 (Cat# S9136S, New England Biolabs) and CLIP-Surface 547 (Cat# S9233S, New England Biolabs) for 45 min at 37°C, in the presence of 10 μg ml^{-1} of Fc-silent MAbs. Cells were then fixed with 4% paraformaldehyde (Cat# 22023, Biotium) and washed, prior to the FRET assay. Images were acquired with an LSM710 confocal microscope (Carl Zeiss) by exciting CLIP-Surface 547 (energy donor) at 543 nm and SNAP-Surface Alexa Fluor 647 (energy acceptor) at 635 nm. Images before and after acceptor bleaching were acquired for FRET efficiency analysis, using ImageJ (Fiji) with the AccPbFRET plugin, as previously described[31, 41].

LUV reconstitution assay

Large unilamellar vesicle (LUV) reconstitution followed by FRET assay was performed as described[30]. For LUV preparation, 80% 1-palmitoyl-2-oleoyl-glycero-3-phosphocholine (POPC, Cat# 850457C, Avanti Polar Lipids) and 20% 1,2-dioleoyl-sn-glycero-3-[(N-(5-amino-1-carboxypentyl)iminodiacetic acid)succinyl] (nickel salt) (DGS-NTA-Ni, Cat# 790404C, Avanti Polar Lipids) were mixed in chloroform, dried under a stream of nitrogen, desiccated for 1 hour in a vacuum container and then resuspended in PBS. LUVs were generated by extrusion 20 times through a pair of polycarbonate filters containing pores of 200 nm diameter. 8.3 nM SNAP-Cell-505-labeled mSLAMF7-His or hPD-L1-His was mixed with 0.23 nM LUVs harboring DGS-NTA-Ni in PBS containing 1.5 mg ml^{-1} BSA and 1 mM tris(2-carboxyethyl)phosphine (TCEP) in a 96-well solid black microplate, during which the SNAP-Cell-505 fluorescence was monitored in real time, using a plate reader with 504-nm excitation and 540-nm emission. After 30 min, the fluorescence reading was paused, and the second protein component, that is 25 nM SNAP-Cell-TMR-labeled mCD47-His or hPD-1-His, was injected and the fluorescence was monitored for another 30 min. For some conditions, SNAP-Cell-505-labeled mCD47-His or SNAP-Cell-TMR-labeled mSLAMF7-His was incubated with Fc-silent MAbs (three-fold molar excess) for 30 min before being added to the reaction. Data were normalized for the mean fluorescence intensity of the last

10 data points, before the addition of SNAP-Cell-TMR-labeled protein, and plotted with GraphPad Prism.

Statistical analyses

Prism 9 software (GraphPad) was used for paired or unpaired Student's t tests (two-tailed), and for one-way ANOVA followed by Tukey's or Dunnett's multiple comparison tests, when appropriate. The normal distribution of the data was tested using the D'Agostino-Pearson normality test (Prism 9) and parametric tests used for statistical analyses accordingly.

Extended Data

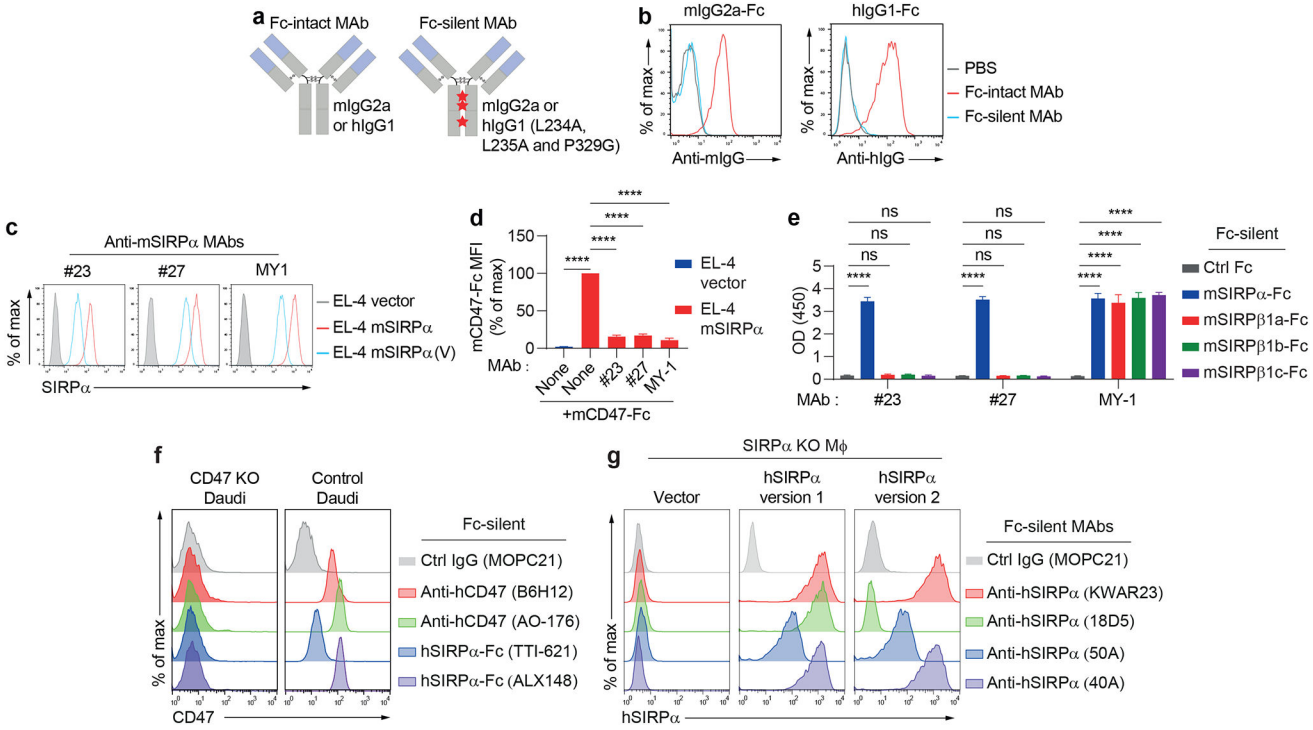

Extended Data Fig. 1. Generation of Fc-silent MAbs and anti-SIRPα MAbs.

a, The three mutations ("LALAPG") introduced in the Fc portion of MAbs to render them Fc-silent are depicted. LALAPG is: L234A ("LA"), leucine 234-to-alanine 234; L235A ("LA"), leucine 235-to-alanine 235; P329G ("PG"), proline 329-to-glycine 329. **b**, Binding of Fc-intact and Fc-silent variants of mIgG2a (MAb MOPC21) or hIgG1 (MAb Z10) to FcRs on BMDMs was assessed by flow cytometry. **c**, Binding of anti-mSIRPα MAbs #23, #27 and MY-1 to EL-4 cells expressing full-length mSIRPα (red lines) or a variant of mSIRPα containing only the first Ig-like variable (V) domain (blue lines) was assessed by flow cytometry. Grey lines, SIRPα-negative cells. **d**, The ability of anti-mSIRPα MAbs to block binding of a soluble mCD47-Fc fusion protein to EL-4 cells, expressing or not expressing mSIRPα, was studied by flow cytometry. MFI, mean fluorescence intensity. **e**, Binding of anti-mSIRPα MAbs to mSIRPα-Fc and 3 known isoforms of mSIRPβ1 (a,b,c), an activating receptor related to SIRPα, was determined by ELISA. MY-1, but not #23 and #27, also bound to SIRPβ1. **f**, Binding of Fc-silent anti-hCD47 MAbs or hSIRPα-

Fc fusion proteins to CD47 KO and CD47-positive Daudi cells was evaluated by flow cytometry. **g**, Binding of Fc-silent anti-hSIRPα MAbs to SIRPα KO BMDMs, transduced with retroviruses encoding or not encoding the V1 or V2 version of hSIRPα, was evaluated by flow cytometry. These two variants are the most common variants of SIRPα found in the human population. Some MAbs such as 18D5 recognize only V1.

All data are means ± s.e.m. ****$p < 0.0001$. Flow cytometry profiles are representative of 3 (**c**,**f**, **g**) or 2 (**b**) independent experiments. Results are pooled from 5 (**d**) and 3 (**e**) independent experiments.

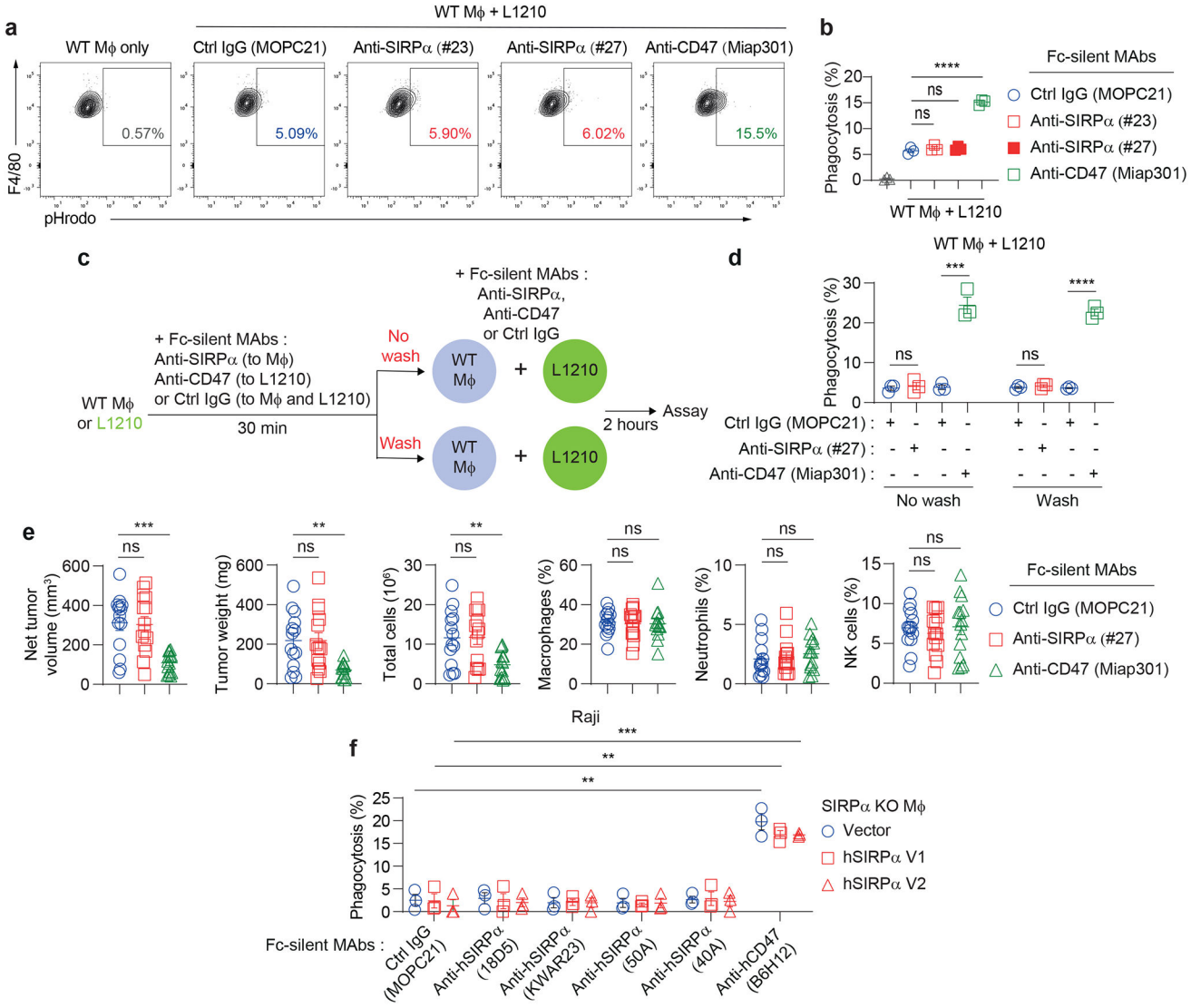

Extended Data Fig. 2. *In vitro* phagocytosis assay and sub-cutaneous tumor transplantation assay.

a,**b**, Same as Fig. 1b, except that phagocytosis was assessed by flow cytometry using the pHrodo dye. A representative experiment is shown in (**a**), and quantification of multiple experiments is depicted in (**b**). Cells with percentages (%) displaying enhanced staining with pHrodo are boxed. **c**,**d**, Same as Fig. 1b, except that macrophages and L1210 cells

were pre-treated with indicated MAbs, followed by extensive washing to remove unbound antibodies prior to the phagocytosis assay. **e**, Tumors from the experiment depicted in Fig. 1g were dissected, weighed, measured and analysed by flow cytometry. Macrophages were $CD11b^+F4/80^+$; neutrophils were $CD11b^+Ly6G^+$; and NK cells were $NK1.1^+$. **f**, Same as Fig. 1h, except that SIRPα KO BMDMs, expressing or not expressing hSIRPα version V1 or V2, and Raji as target, were used.

All data are means ± s.e.m. ns, not significant; $^{**}p < 0.01$, $^{***}p < 0.001$, and $^{****}p < 0.0001$. Flow cytometry profiles are representative of 3 (**a**) independent experiments. Results are pooled from 3 (**b**,**d**,**f**) mice studied in independent experiments or 14 (**e**) mice from 3 independent experiments. Each symbol represents one mouse.

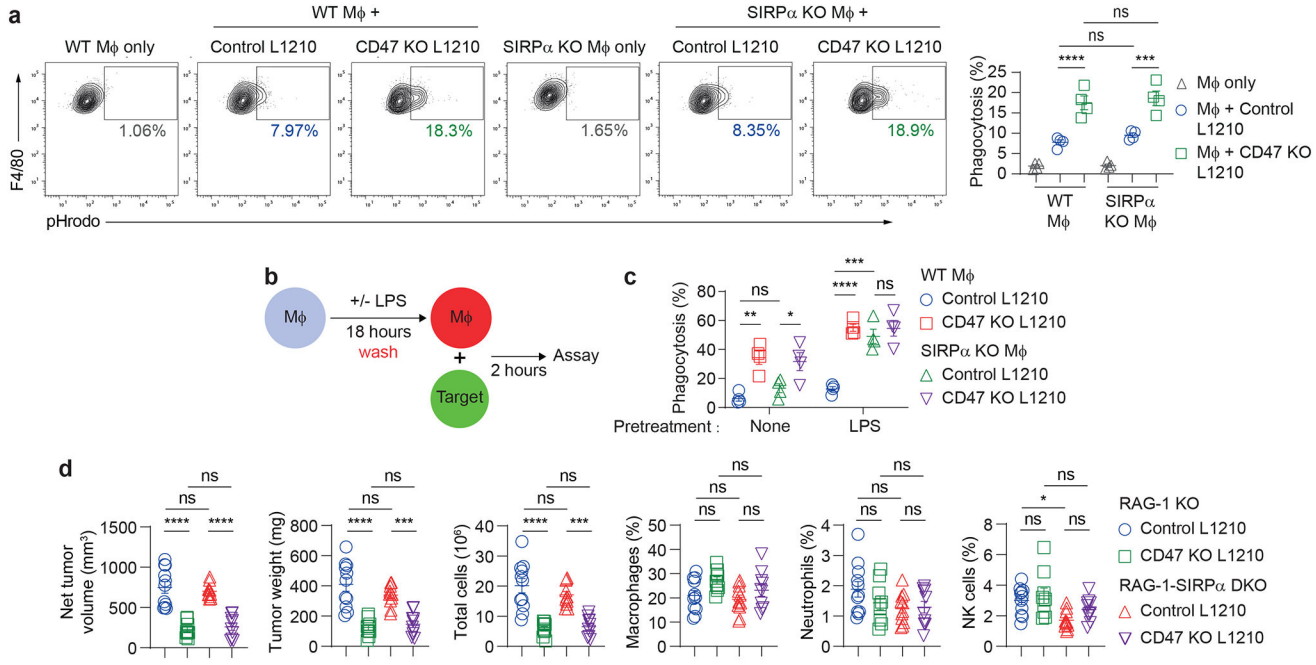

Extended Data Fig. 3. pHrodo-based phagocytosis assays, phagocytosis assays in an inflammatory setting, and *in vivo* tumor formation assays.

a, Same as Fig. 2a, except that phagocytosis was assessed by flow cytometry using the pHrodo dye. A representative experiment is shown on the left and quantification of multiple experiments is depicted on the right. Cells with percentages (%) displaying enhanced staining with pHrodo are boxed. **b**,**c**, Same as Fig. 2a, except that macrophages were pre-treated with or without lipopolysaccharide (LPS). **d**, Tumors from the experiment depicted in Fig. 2f were dissected, weighed, measured and analysed by flow cytometry. Macrophages were $CD11b^+F4/80^+$; neutrophils were $CD11b^+Ly6G^+$; and NK cells were $NK1.1^+$. One mouse from "RAG-1 KO mice plus CD47 KO L1210" group showed no clinically detectable tumor on day 17.

Data are means ± s.e.m. ns, not significant; $^{*}p < 0.05$, $^{***}p < 0.001$, and $^{****}p < 0.0001$. Flow cytometry profiles are representative of 4 independent experiments. Results are pooled from a total of 4 (**a**,**c**) mice studied in independent experiments or 11 (control L1210) or 10 (CD47 KO L1210) mice from 2 independent experiments (**d**). Each symbol represents one mouse.

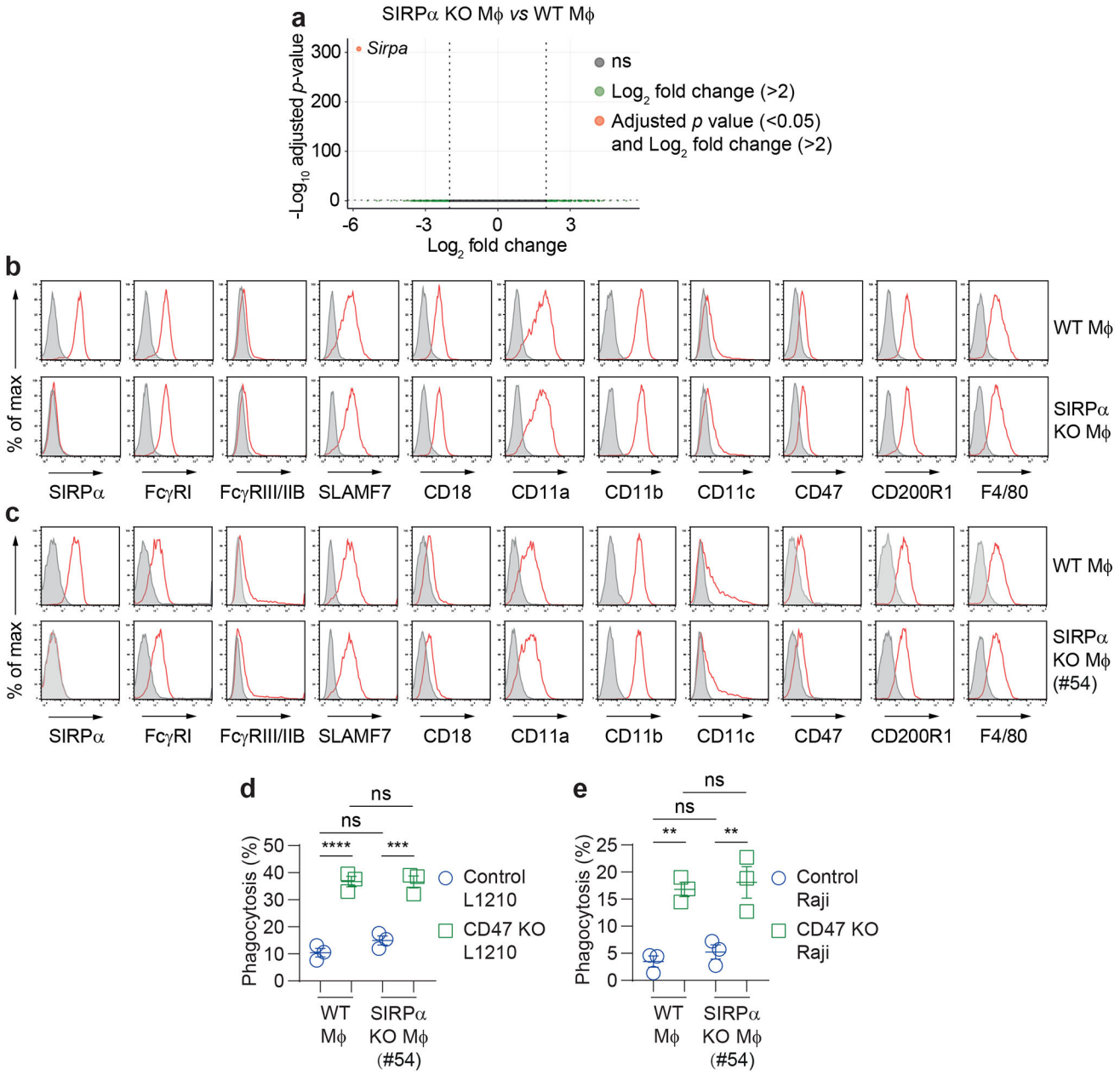

Extended Data Fig. 4. Loss of SIRPα does not alter macrophage differentiation.

a, Volcano plot of gene expression differences between SIRPα KO *vs* WT BMDMs is depicted. RNA from BMDMs was processed for RNA-Seq library preparation. Differential expression analysis was performed with DESeq2 v1.14.1 from the raw alignment counts calculated with FeatureCounts v1.4.6. Differentially expressed genes were defined as genes with an adjusted *p* value of < 0.05 and a $\log_2$ fold change of greater or equal to 1.0 (X axis). $-\log_{10}$ *p* value is shown on Y axis. **b**, Expression of various cell surface markers (red lines) on BMDMs was evaluated by flow cytometry. Filled curves, Ctrl IgG. **c**, Same as b, except that BMDMs from a second independent SIRPα KO mouse strain (#54) were studied. **d**,**e**, Same as Fig. 2a, except that BMDMs from a second independent SIRPα KO mouse strain #54 were studied.

All data are means ± s.e.m. ns, not significant; $^{**}p < 0.01$, $^{***}p < 0.001$, and $^{****}p < 0.0001$. 3 pairs of mice were studied in one experiment (**a**). Flow cytometry profiles are representative of 3 (**b**,**c**) independent experiments. Results are pooled from a total of 3 (**d**,**e**) mice studied in 3 independent experiments. Each symbol represents one mouse.

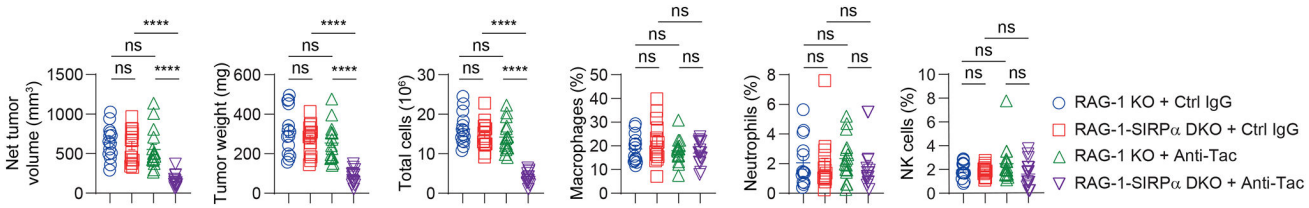

Extended Data Fig. 5. Loss of SIRPα in mice promotes FcR-mediated tumor growth inhibition.

Tumors from the experiment depicted in Fig. 3f were dissected, weighed, measured and analysed by flow cytometry. Macrophages were $CD11b^{+}F4/80^{+}$; neutrophils were $CD11b^{+}Ly6G^{+}$; and NK cells were $NK1.1^{+}$. One mouse from "RAG-1 KO plus Ctrl IgG" group showed no clinically detectable tumor on day 18.

All data are means ± s.e.m. ns, not significant; $^{****}p < 0.0001$. Results are pooled from a total of 15 mice (16 mice for "RAG-1 KO plus 7G7" group) from 3 independent experiments. Each symbol represents one mouse.

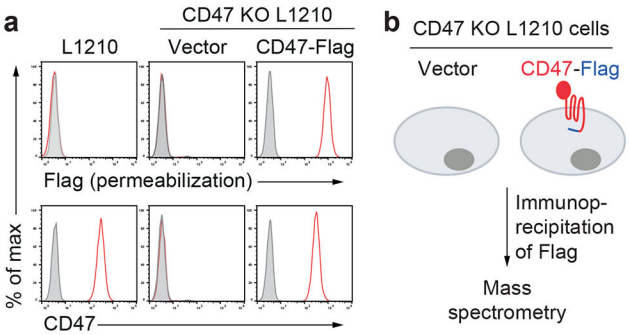

c

Normalized Total TIC			Normalized Total TIC		
Protein	CD47-Flag	Vector	Protein	CD47-Flag	Vector
SLAMF7	9.07E+05	0.00E+00	UQCRC2	2.74E+04	0.00E+00
CD47	4.67E+05	0.00E+00	RPL18A	2.54E+04	0.00E+00
RPS4X	5.37E+04	0.00E+00	SLC25A12	2.18E+04	0.00E+00
CHIA	4.35E+04	0.00E+00	RPL21	1.60E+04	0.00E+00
RPL13	4.18E+04	0.00E+00	RPN1	1.53E+04	0.00E+00
RPS3A1	3.87E+04	0.00E+00	PA2G4	7.25E+03	0.00E+00
RPS14	3.48E+04	0.00E+00	SERBP1	6.22E+03	0.00E+00

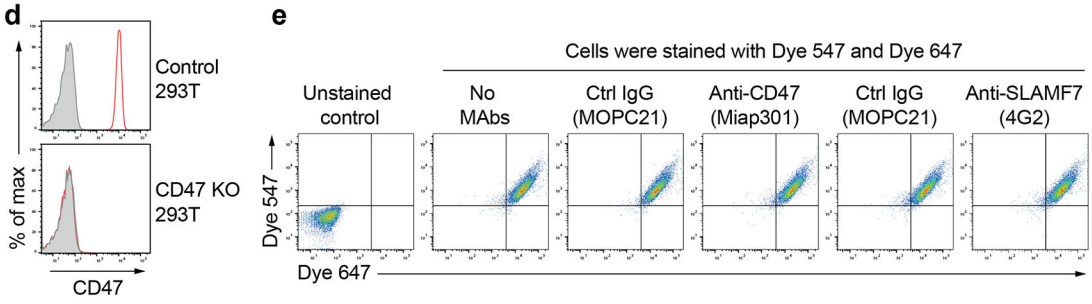

Extended Data Fig. 6. CD47 interacts with SLAMF7.

a, Expression of Flag or CD47 (red lines) on L1210 and CD47 KO L1210 cells expressing or not expressing mCD47-Flag was assessed by flow cytometry. Permeabilization was used for the anti-Flag staining. Filled curves, Ctrl IgG. **b**,**c**, Same as Fig. 4b. A schematic representation of the protocol used for mass spectrometry is depicted in (**b**). Means of the normalized total ion current (TIC) for the potential interactors are shown in (**c**). **d**, Expression of hCD47 (red lines) on control or CD47 KO 293T cells was assessed by flow

cytometry. Filled curves, Ctrl IgG. **e**, After transfection with tagged versions of CD47 and SLAMF7, CD47 KO 293T cells were stained with Dye 647 and Dye 547 in the presence or absence of Ctrl IgG, anti-CD47 MAb, or anti-SLAMF7 MAb. The fluorescence intensity of Dye 647 and Dye 547 was assayed by flow cytometry.

Flow cytometry profiles are representative of 3 (**a**,**d**,**e**) independent experiments. Results are pooled from 3 (**c**) independent experiments.

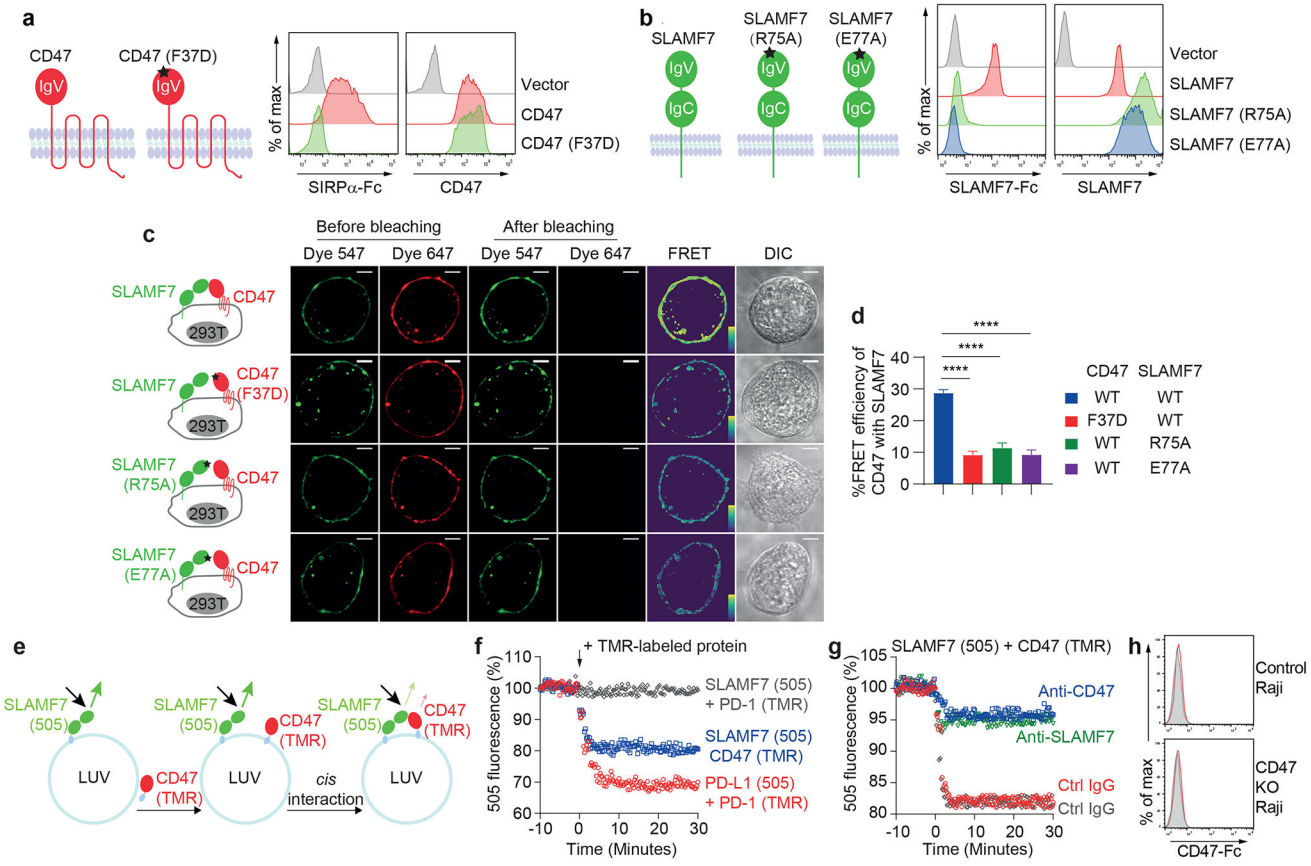

Extended Data Fig. 7. CD47 interacts in *cis* with SLAMF7.

a, Binding of soluble mSIRPα-Fc fusion protein and expression of mCD47 on transfected CD47 KO 293T cells were assessed by flow cytometry. **b**, Binding of soluble mSLAMF7-Fc fusion protein and expression of mSLAMF7 on transfected BI-141 cells were assessed by flow cytometry. **c**,**d**, Same as Fig. 4d,e, except that CD47 KO 293T cells were transfected with a variety of mSLAMF7 and mCD47 constructs. **e-g**, LUV-based FRET assay. Recombinant histidine-tagged versions of the extracellular domain of mCD47 and mSLAMF7, coupled to different fluorophores (Dye 505 for SLAMF7 as donor and Dye TMR for CD47 as acceptor) were sequentially added to nickel-containing LUVs. Changes in donor fluorescence were analyzed over time. (**e**) Schematic representation of assay. (**f**) Time-course of normalized dye 505 fluorescence intensity for mSLAMF7 or hPD-L1. The interaction of hPD-1 and hPD-L1 was used as a positive control. (**g**) Same as g, except that blocking anti-mCD47, blocking anti-mSLAMF7 or control MAbs were added 30 min

before the LUV FRET assay. (h) Binding of soluble hCD47-Fc fusion protein on transfected control or CD47 KO Raji cells were assessed by flow cytometry.

All data are means ± s.e.m. ns, not significant; ****$p < 0.0001$. Flow cytometry profiles are representative of 3 (**a**,**b**) or 2 (**h**) independent experiments. Results are representative of 3 (**c**,**f**) or 2 (**g**) independent experiments. Results are pooled from 3 (**d**) independent experiments.

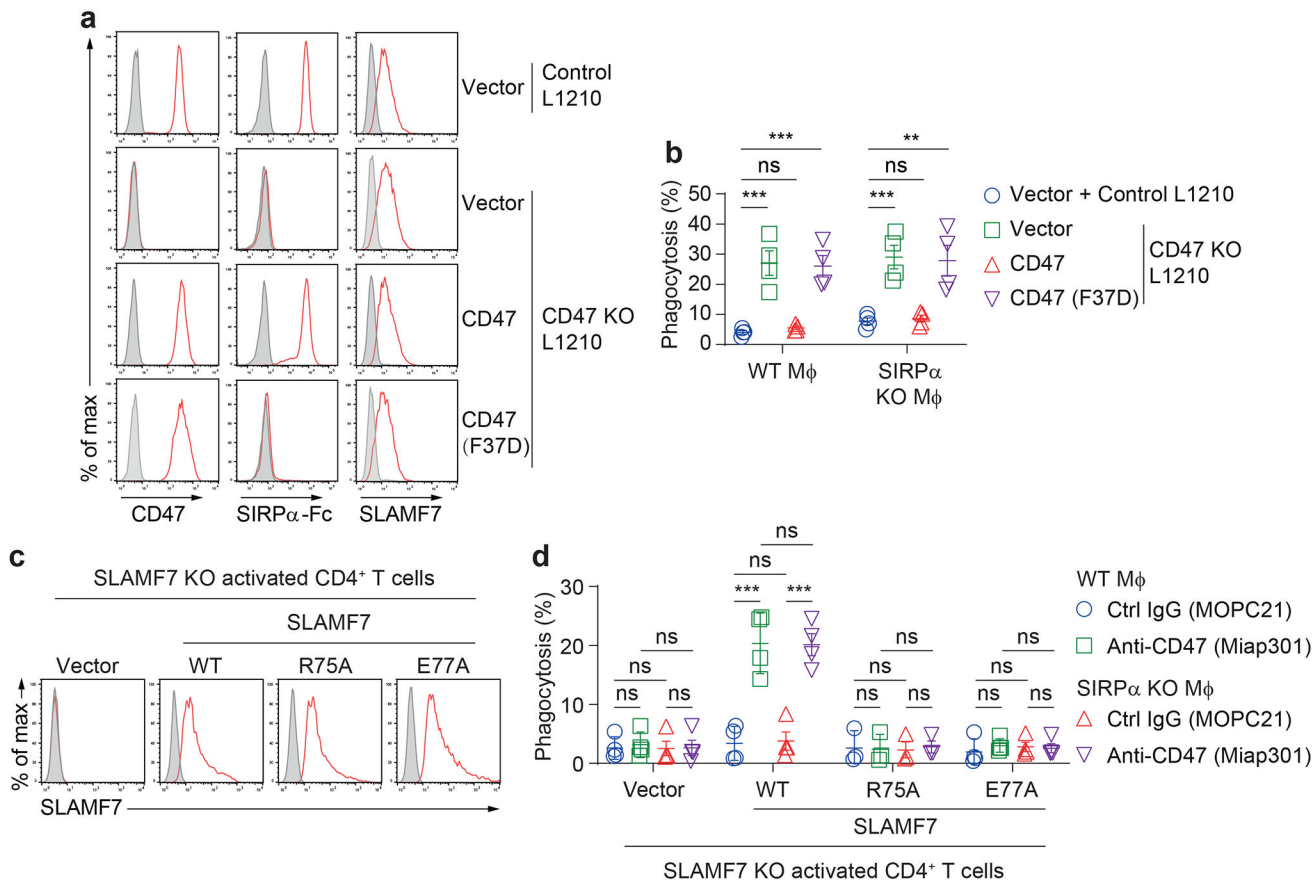

Extended Data Fig. 8. Structure-function analyses of CD47 and SLAMF7.

a, Expression of mCD47 and mSLAMF7 and binding of mSIRPα-Fc (red lines) on L1210 derivatives were assessed by flow cytometry. Filled curves, Ctrl IgG or Fc fusion protein. **b**, Same as Fig. 2a, using a variety of L1210 derivatives as targets. **c**, Expression of mSLAMF7 (red lines) on SLAMF7 KO activated $CD4^+$ T cells transduced with variants of mSLAMF7 constructs. Filled curves, Ctrl IgG. **d**, Same as b, but using activated $CD4^+$ T cells expressing variants of mSLAMF7 as targets.

All data are means ± s.e.m. ns, not significant; **$p < 0.01$ and ***$p < 0.001$. Flow cytometry profiles are representative of 3 (**a**,**c**) independent experiments. Results are pooled from 4 (**b**) or 4 (**d**; for all variants, except 3 for R75A) independent experiments. Each symbol represents one mouse.

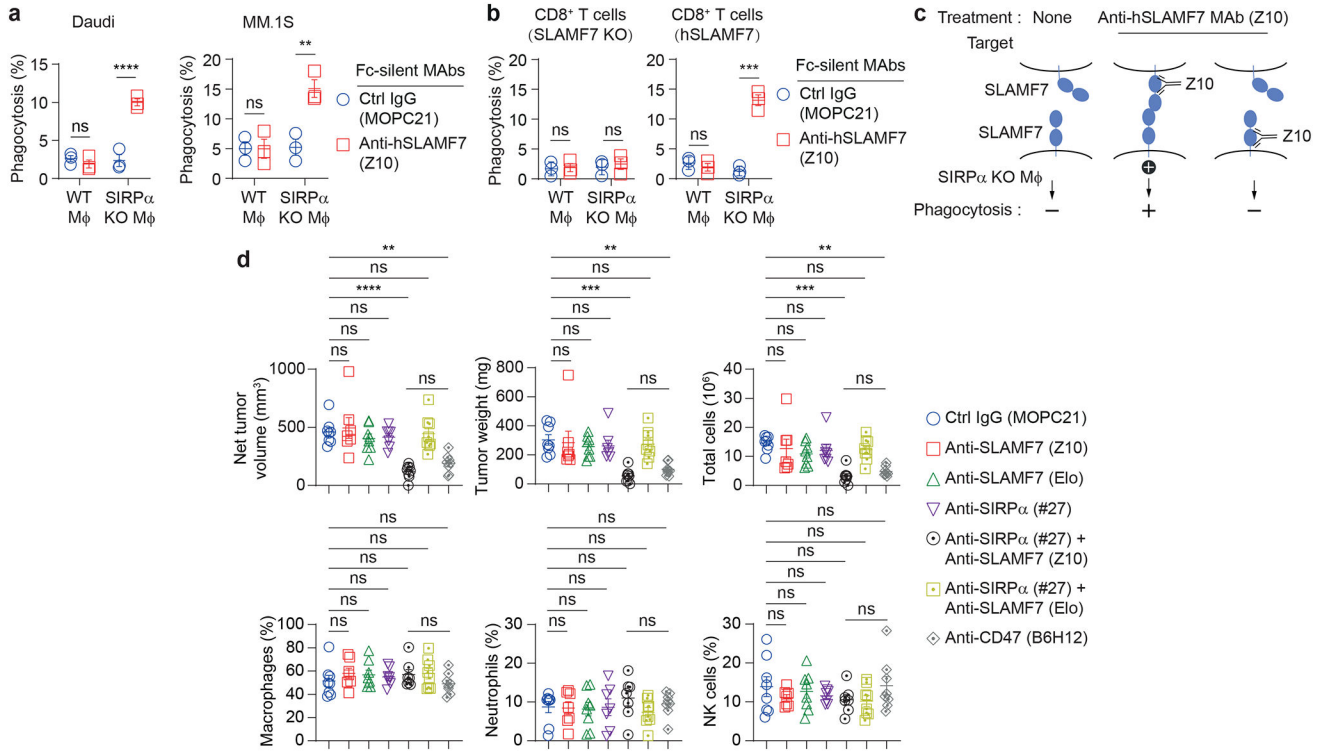

Extended Data Fig. 9. Impact of MAb Z10 on macrophages and targets, and sub-cutaneous tumor transplantation assay.

a,**b**, Same as Fig. 2a, using BMDMs from WT or SIRPα KO mice and Daudi (**a**, left), MM.1S (**a**, right), and activated mouse CD8$^+$ T cells (**b**) expressing or not expressing hSLAMF7 as targets. **c**, Schematic representations of the impact of MAb Z10, depending on whether MAb Z10 binds SLAMF7 on macrophages or target cells. **d**, Tumors from experiment depicted in Fig. 6g were dissected, weighed, measured and analysed by flow cytometry. Macrophages were CD11b$^+$F4/80$^+$; neutrophils were CD11b$^+$Ly6G$^+$; and NK cells were NK1.1$^+$. One mouse showed no detectable tumor in the “anti-SIRPα (#27) plus anti-SLAMF7 (Z10)” group on day 24.

All data are means ± s.e.m. ns, not significant; $^{**}p < 0.01$, $^{***}p < 0.001$, and $^{****}p < 0.0001$. Results are pooled from 3 (**a,b**) mice studied in independent experiments; 8 [except 7 for “anti-SLAMF7 (Z10)” and “anti-SIRPα (#27)” groups] mice from 2 independent experiments (**d**). Each symbol represents one mouse.

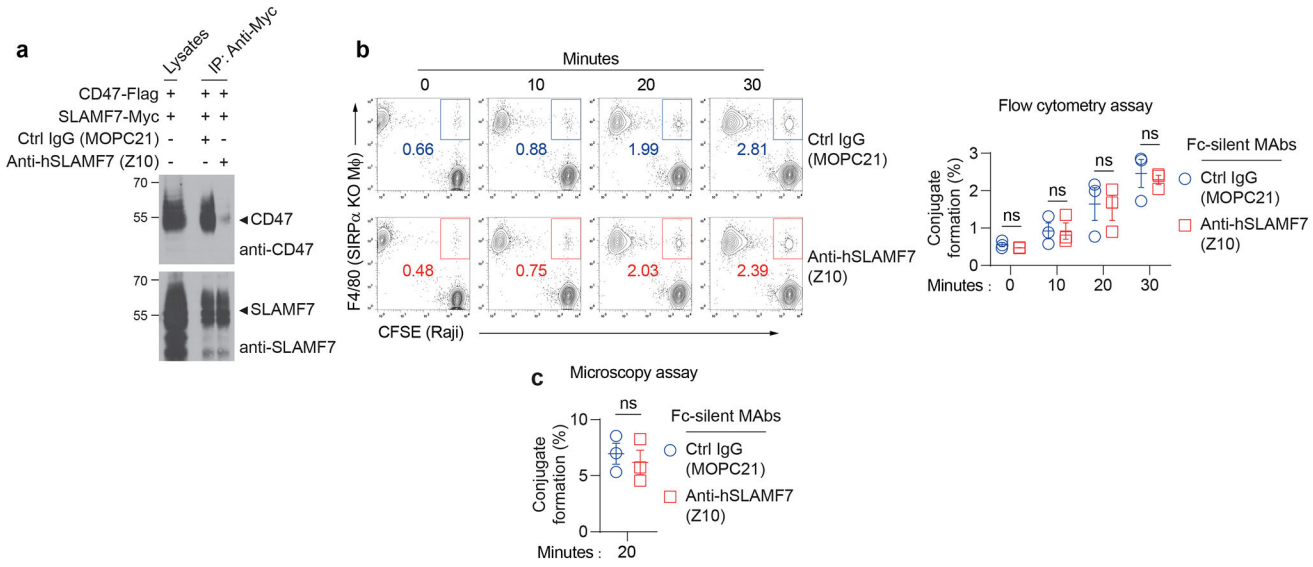

Extended Data Fig. 10. MAb Z10 disrupts CD47 and SLAMF7 interaction and does not affect conjugate formation.

a, Co-immunoprecipitation of CD47 and SLAMF7 in CD47 KO 293T cells expressing a Flag-tagged variant of hCD47 and a Myc-tagged variant of hSLAMF7, in the presence of Ctrl IgG or anti-hSLAMF7 MAb Z10. Flag and Myc tags were added at the carboxyl terminus of hCD47 or hSLAMF7, respectively. The abundance of the transfected proteins in total cell lysates was analyzed in parallel. IP, immunoprecipitation. **b**, Formation of conjugates (boxed) between SIRPα KO BMDMs and Raji, in presence of Ctrl IgG or anti-hSLAMF7 MAb Z10, was detected by flow cytometry. Left, representative experiment. The percentages of conjugate formation are indicated below the boxes. Right, quantification of multiple independent experiments. **c**, Same as b, except that conjugates were assessed by confocal microscopy, after 20 min of co-incubation of SIRPα KO BMDMs and Raji. All data are means ± s.e.m. ns, not significant. Results are representative of 2 (**a**) independent experiments. Flow cytometry profiles are representative of 3 independent experiments (**b**). Results are pooled from a total of 3 (**b**,**c**) mice studied in independent experiments. Each symbol represents one mouse.

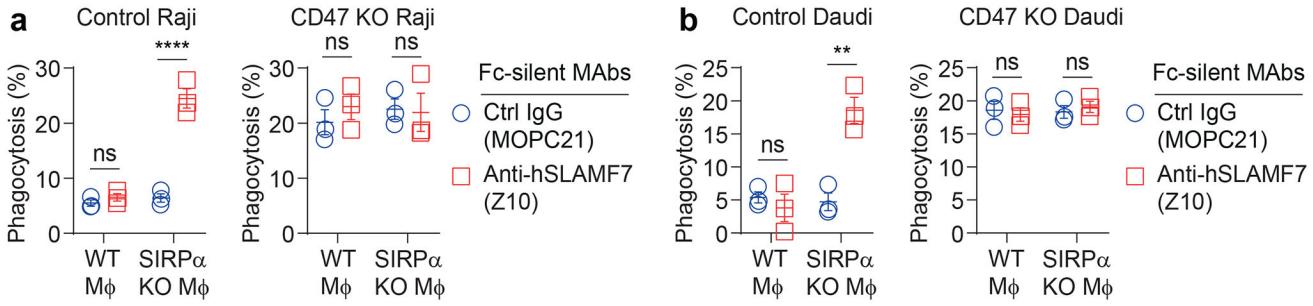

Extended Data Fig. 11. MAb Z10 does not interfere with phagocytosis of CD47 KO targets.

a,**b**, Same as Fig. 6a, except that BMDMs from WT or SIRPα KO mice and the indicated target cells, expressing or not expressing hCD47 [Raji (**a**), Daudi (**b**)] were studied.

All data are means ± s.e.m. ns, not significant; $^{**}p < 0.01$ and $^{****}p < 0.0001$. Results are pooled from 3 (**a**,**b**) mice studied in 3 independent experiments. Each symbol represents one mouse.

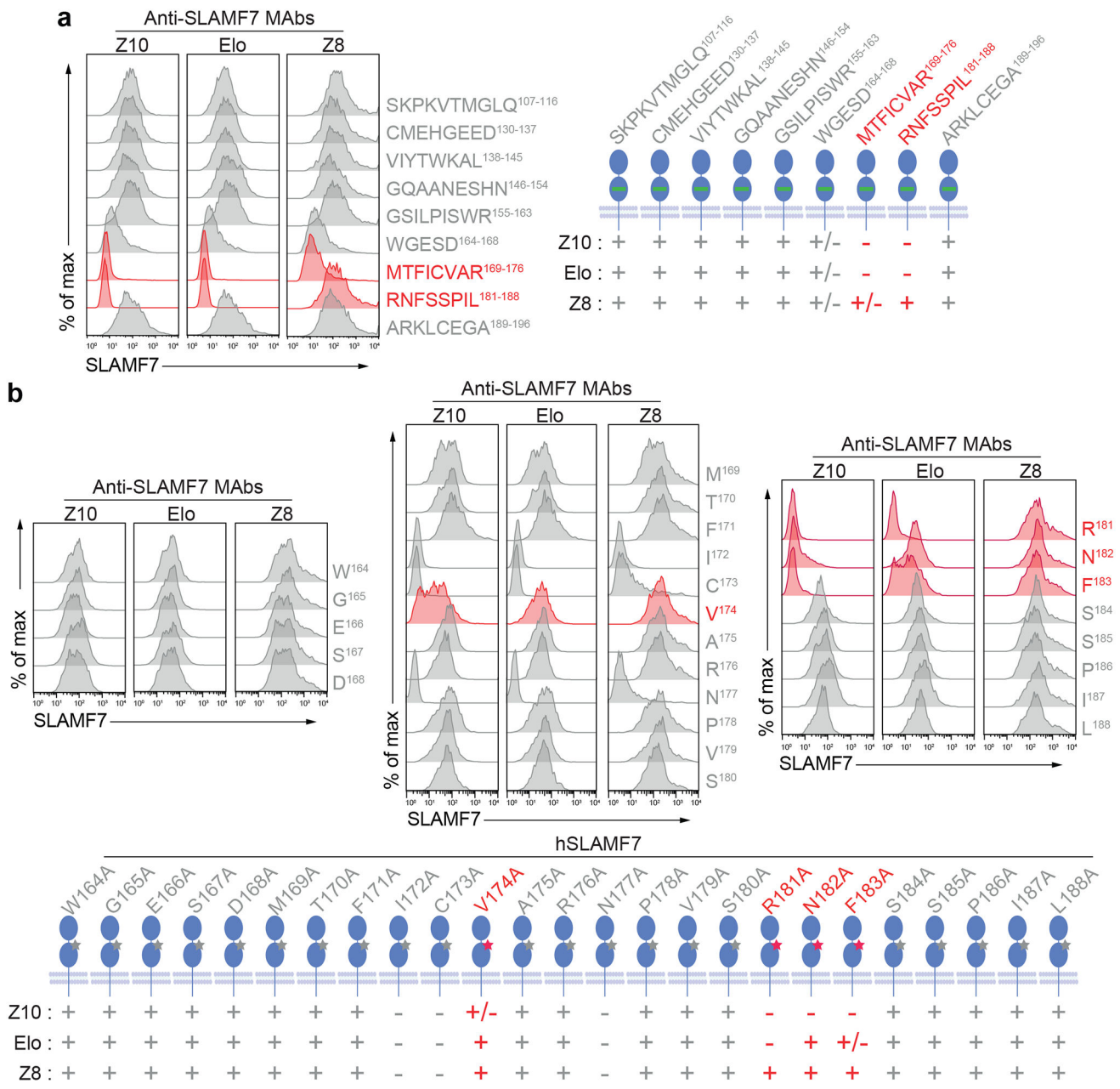

Extended Data Fig. 12. MAb Z10 binds to the second Ig-like domain of SLAMF7.

a,**b**, Binding of anti-hSLAMF7 MAbs Z10, elotuzumab (Elo) and Z8 to CD47 KO 293T cells, expressing various chimeras between hSLAMF7 and mSLAMF7 (**a**) or various mutants of hSLAMF7 (**b**), was determined by flow cytometry. For the chimeras, the residues in hSLAMF7 (numbered) were replaced by the equivalent residues in mSLAMF7. For the point mutants, residues were replaced by alanines. +, binding; +/−, partial binding; -, no binding. Asterisks indicate the site of the mutation.

Flow cytometry profiles are representative of 3 (**a**,**b**, except 2 for N^{177}, P^{178}, V^{179}, S^{180}) independent experiments.

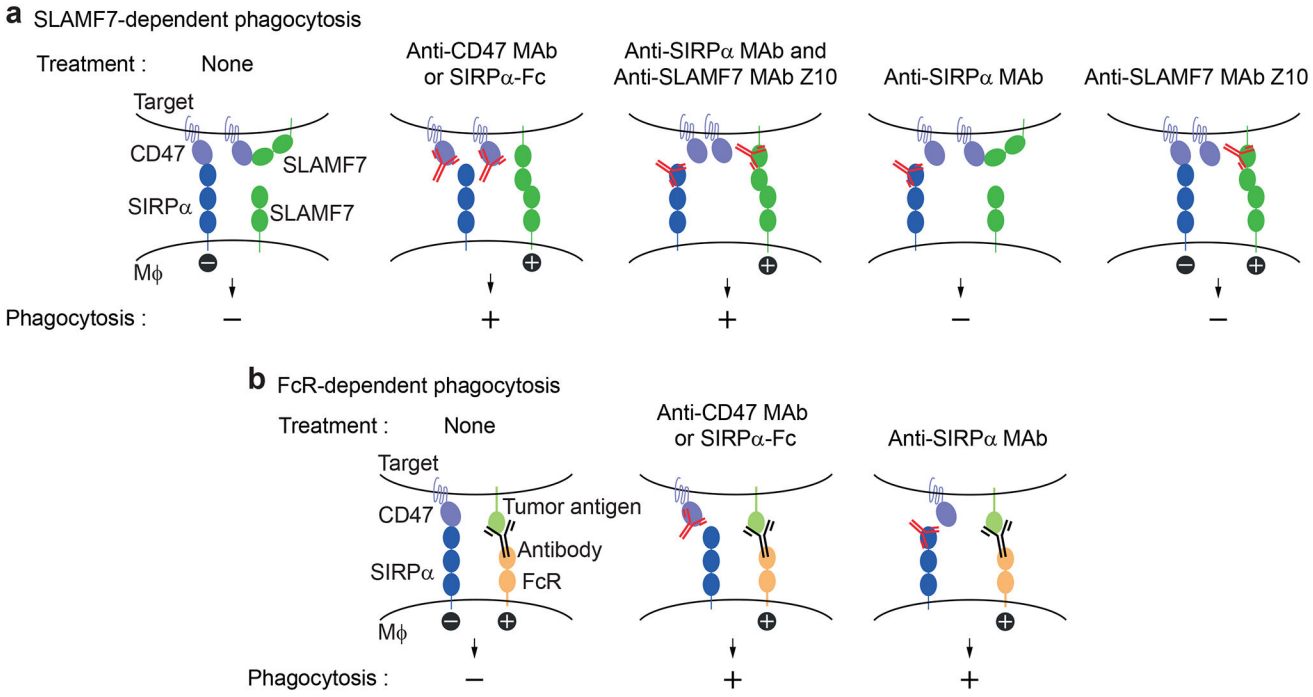

Extended Data Fig. 13. Impact of CD47 blockade, SIRPα blockade and agonistic anti-SLAMF7 MAb on phagocytosis.

a,**b**, Models of the effects of CD47 blockade, SIRPα blockade and agonistic anti-SLAMF7 MAb Z10 on phagocytosis of SLAMF7-positive (**a**) and antibody-opsonized (**b**) tumor cells are depicted. +, phagocytosis; -, no phagocytosis.

Acknowledgements

We thank members of the Veillette laboratory for useful discussions. We also acknowledge T. van den Berg (Amsterdam, The Netherlands) and T. Matozaki (Kobe, Japan) for providing hybridomas. This work was supported by grants from the Canadian Institutes of Health Research (MT-14429, MOP-82906, FDN-143338, PJT-178314 and PJT-183593), the Terry Fox Research Institute (1190-02) and the Ministère de l'économie et de l'innovation (MEI; Québec) to A.V.; and US National Institutes of Health grant R37 CA239072 to E.H. A.V. received a contract from Bristol Myers-Squibb to study the mechanism of action of anti-SLAMF7 monoclonal antibody elotuzumab against multiple myeloma. Z.T. received a Fellowship from the Cole Foundation; C.C.G. receives a Studentship from the Fonds de la recherche en santé – Québec; J.L. receives a Studentship from the Chinese Science Council; and A.V. holds the Canada Research Chair on Signaling in the Immune System.

Data availability

RNA-Seq data supporting the findings of this study have been deposited into the Gene Expression Omnibus (GEO) database under accession number GSE223059. All other relevant data are available from the corresponding author upon reasonable request.

References

1. Minn AJ & Wherry EJ Combination Cancer Therapies with Immune Checkpoint Blockade: Convergence on Interferon Signaling. Cell 165, 272–275 (2016). [PubMed: 27058661]

2. Sharma P & Allison JP Dissecting the mechanisms of immune checkpoint therapy. Nat Rev Immunol 20, 75–76 (2020). [PubMed: 31925406]
3. Son J et al. Inhibition of the CD47-SIRPalpha axis for cancer therapy: A systematic review and meta-analysis of emerging clinical data. Front Immunol 13, 1027235 (2022). [PubMed: 36439116]
4. Veillette A & Chen J SIRPalpha-CD47 Immune Checkpoint Blockade in Anticancer Therapy. Trends Immunol 39, 173–184 (2018). [PubMed: 29336991]
5. Chen J et al. SLAMF7 is critical for phagocytosis of haematopoietic tumour cells via Mac-1 integrin. Nature 544, 493–497 (2017). [PubMed: 28424516]
6. Chao MP et al. Anti-CD47 antibody synergizes with rituximab to promote phagocytosis and eradicate non-Hodgkin lymphoma. Cell 142, 699–713 (2010). [PubMed: 20813259]
7. Advani R et al. CD47 Blockade by Hu5F9-G4 and Rituximab in Non-Hodgkin's Lymphoma. N Engl J Med 379, 1711–1721 (2018). [PubMed: 30380386]
8. Feng M et al. Phagocytosis checkpoints as new targets for cancer immunotherapy. Nat Rev Cancer 19, 568–586 (2019). [PubMed: 31462760]
9. Matlung HL, Szilagyi K, Barclay NA & van den Berg TK The CD47-SIRPα signaling axis as an innate immune checkpoint in cancer. Immunological reviews 276, 145–164 (2017). [PubMed: 28258703]
10. Zhao XW et al. CD47-signal regulatory protein-alpha (SIRPalpha) interactions form a barrier for antibody-mediated tumor cell destruction. Proc Natl Acad Sci U S A 108, 18342–18347 (2011). [PubMed: 22042861]
11. Zhao XW, Kuijpers TW & van den Berg TK Is targeting of CD47-SIRPα enough for treating hematopoietic malignancy? Blood, The Journal of the American Society of Hematology 119, 4333–4334 (2012).
12. Petrova PS et al. TTI-621 (SIRPalphaFc): A CD47-Blocking Innate Immune Checkpoint Inhibitor with Broad Antitumor Activity and Minimal Erythrocyte Binding. Clin Cancer Res 23, 1068–1079 (2017). [PubMed: 27856600]
13. Weiskopf K et al. Engineered SIRPalpha variants as immunotherapeutic adjuvants to anticancer antibodies. Science 341, 88–91 (2013). [PubMed: 23722425]
14. Ring NG et al. Anti-SIRPalpha antibody immunotherapy enhances neutrophil and macrophage antitumor activity. Proc Natl Acad Sci U S A 114, E10578–E10585 (2017). [PubMed: 29158380]
15. Tang Z et al. Inflammatory macrophages exploit unconventional pro-phagocytic integrins for phagocytosis and anti-tumor immunity. Cell Rep 37, 110111 (2021). [PubMed: 34910922]
16. Guo H, Cruz-Munoz ME, Wu N, Robbins M & Veillette A Immune cell inhibition by SLAMF7 is mediated by a mechanism requiring src kinases, CD45, and SHIP-1 that is defective in multiple myeloma cells. Mol Cell Biol 35, 41–51 (2015). [PubMed: 25312647]
17. Lu Y et al. Immunological conversion of solid tumours using a bispecific nanobioconjugate for cancer immunotherapy. Nat Nanotechnol (2022).
18. Johnson LDS et al. Targeting CD47 in Sezary syndrome with SIRPalphaFc. Blood Adv 3, 1145–1153 (2019). [PubMed: 30962222]
19. Querfeld C et al. Intralesional TTI-621, a novel biologic targeting the innate immune checkpoint CD47, in patients with relapsed or refractory mycosis fungoides or Sezary syndrome: a multicentre, phase 1 study. Lancet Haematol 8, e808–e817 (2021). [PubMed: 34627593]
20. Strati P et al. Interim Results from the First Clinical Study of CC-95251, an Anti-Signal Regulatory Protein-Alpha (SIRPα) Antibody, in Combination with Rituximab in Patients with Relapsed and/or Refractory Non-Hodgkin Lymphoma (R/R NHL). Blood 138, 2493 (2021).
21. Delidakis G, Kim JE, George K & Georgiou G Improving antibody therapeutics by manipulating the Fc domain: immunological and structural considerations. Annual review of biomedical engineering 24, 249–274 (2022).
22. Kang TH & Jung ST Boosting therapeutic potency of antibodies by taming Fc domain functions. Experimental & molecular medicine 51, 1–9 (2019).
23. Lo M et al. Effector-attenuating Substitutions That Maintain Antibody Stability and Reduce Toxicity in Mice. J Biol Chem 292, 3900–3908 (2017). [PubMed: 28077575]

24. Bian Z et al. Cd47-Sirpα interaction and IL-10 constrain inflammation-induced macrophage phagocytosis of healthy self-cells. Proceedings of the National Academy of Sciences 113, E5434–E5443 (2016).
25. Sekar RB & Periasamy A Fluorescence resonance energy transfer (FRET) microscopy imaging of live cell protein localizations. The Journal of cell biology 160, 629 (2003). [PubMed: 12615908]
26. Cao E et al. NTB-A receptor crystal structure: insights into homophilic interactions in the signaling lymphocytic activation molecule receptor family. Immunity 25, 559–570 (2006). [PubMed: 17045824]
27. Hatherley D et al. Paired receptor specificity explained by structures of signal regulatory proteins alone and complexed with CD47. Mol Cell 31, 266–277 (2008). [PubMed: 18657508]
28. Goyette M-A et al. The receptor tyrosine kinase AXL is required at multiple steps of the metastatic cascade during HER2-positive breast cancer progression. Cell reports 23, 1476–1490 (2018). [PubMed: 29719259]
29. Blanchard EL et al. Proximity ligation assays for in situ detection of innate immune activation: focus on in vitro-transcribed mRNA. Molecular Therapy-Nucleic Acids 14, 52–66 (2019). [PubMed: 30579042]
30. Zhao Y et al. Antigen-Presenting Cell-Intrinsic PD-1 Neutralizes PD-L1 in cis to Attenuate PD-1 Signaling in T Cells. Cell Rep 24, 379–390 e376 (2018). [PubMed: 29996099]
31. Zhao Y et al. PD-L1:CD80 Cis-Heterodimer Triggers the Co-stimulatory Receptor CD28 While Repressing the Inhibitory PD-1 and CTLA-4 Pathways. Immunity 51, 1059–1073 e1059 (2019). [PubMed: 31757674]
32. Zhao Y et al. cis-B7: CD28 interactions at invaginated synaptic membranes provide CD28 co-stimulation and promote CD8+ T cell function and anti-tumor immunity. Immunity (2023).
33. Ritchie D & Colonna M Mechanisms of Action and Clinical Development of Elotuzumab. Clin Transl Sci 11, 261–266 (2018). [PubMed: 29272564]
34. Howden AJM et al. Quantitative analysis of T cell proteomes and environmental sensors during T cell differentiation. Nat Immunol 20, 1542–1554 (2019). [PubMed: 31591570]
35. Guo H et al. Deletion of Slam locus in mice reveals inhibitory role of SLAM family in NK cell responses regulated by cytokines and LFA-1. J Exp Med 213, 2187–2207 (2016). [PubMed: 27573813]
36. Abraham N, Miceli MC, Parnes JR & Veillette A Enhancement of T-cell responsiveness by the lymphocyte-specific tyrosine protein kinase p56lck. Nature 350, 62–66 (1991). [PubMed: 1706070]
37. Bouchon A, Cella M, Grierson HL, Cohen JI & Colonna M Activation of NK cell-mediated cytotoxicity by a SAP-independent receptor of the CD2 family. J Immunol 167, 5517–5521 (2001). [PubMed: 11698418]
38. von Boehmer L et al. Sequencing and cloning of antigen-specific antibodies from mouse memory B cells. Nat Protoc 11, 1908–1923 (2016). [PubMed: 27658009]
39. Davidson D et al. The Csk-Associated Adaptor PAG Inhibits Effector T Cell Activation in Cooperation with Phosphatase PTPN22 and Dok Adaptors. Cell Rep 17, 2776–2788 (2016). [PubMed: 27926878]
40. Zhong MC et al. SLAM family receptors control pro-survival effectors in germinal center B cells to promote humoral immunity. J Exp Med 218 (2021).
41. Roszik J, Szollosi J & Vereb G AccPbFRET: an ImageJ plugin for semi-automatic, fully corrected analysis of acceptor photobleaching FRET images. BMC Bioinformatics 9, 346 (2008). [PubMed: 18713453]

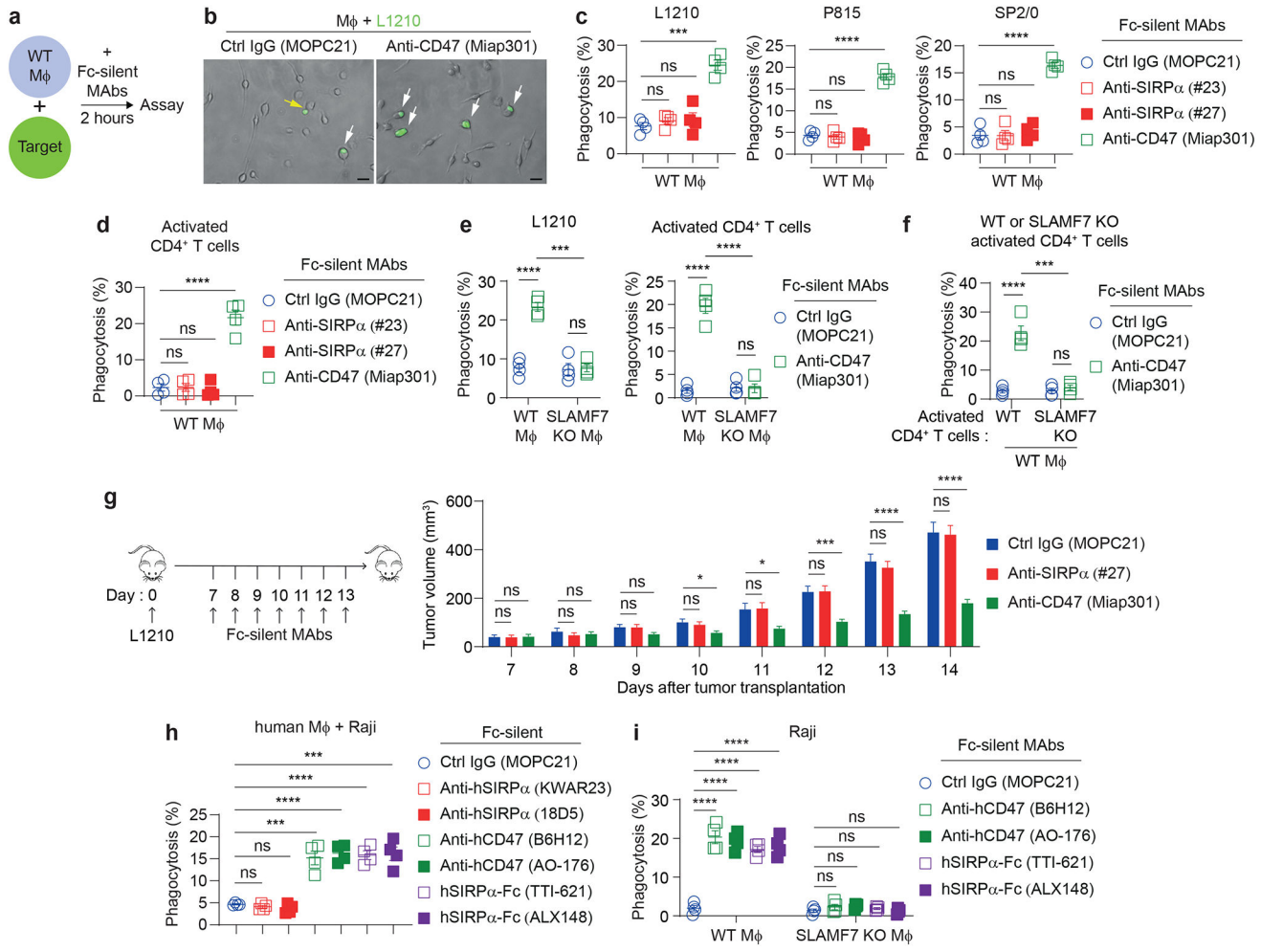

Fig. 1. Blockade of CD47, but not of SIRPα, promotes phagocytosis triggered by pro-phagocytic ligand SLAMF7

a, Schematic representation of phagocytosis assay is shown. Fc, fragment crystallizable. MAbs, monoclonal antibodies. Mϕ, macrophage. **b**,**c**, Phagocytosis of mouse (m) tumor cells L1210, P815 or SP2/0 by wild-type (WT) bone marrow-derived macrophages (BMDMs) in the presence of Fc-silent MAbs was assayed by fluorescence microscopy. Representative photomicrographs of phagocytosis assays are shown in (b). Phagocytosis of L1210 (green) is depicted by white arrows. Conjugate formation of L1210 with BMDMs without phagocytosis is depicted by yellow arrows. Data from multiple mice are shown in (c). Scale bars, 50 μm. Ctrl, control. IgG, immunoglobulin G. The Fc portion of the MAbs was from mIgG2a and carried the "LALAPG" mutation, which prevents Fc receptor-binding. **d**, Same as b, except that activated $CD4^+$ T cells were used as targets. **e**, Same as b, except that WT or SLAMF7 KO BMDMs, as well as L1210 (left) or activated $CD4^+$ T cells (right) as targets, were used. **f**, Same as b, except that WT or SLAMF7 KO activated $CD4^+$ T cells were used as targets. **g**, Sub-cutaneous tumor transplantation assay. Tumor volume over time of L1210 injected sub-cutaneously in RAG-1 KO mice, in the presence of the indicated MAbs (Fc-silent), was measured using a caliper. **h**, Phagocytosis of human (h) Raji lymphoma cells by human blood-derived macrophages in the presence of Fc-silent

blocking MAbs or soluble fusion proteins was assessed by fluorescence microscopy. The Fc portion was from hIgG1 and carried the LALAPG mutation. **i,** Same as h, except that WT or SLAMF7 KO mouse BMDMs were used.

All data are means ± s.e.m. ns, not significant; *$p < 0.05$, ***$p < 0.001$, and ****$p < 0.0001$. Results are pooled from a total of 4 (**c**-**f**,**i**) mice studied in independent experiments; 14 mice from 3 independent experiments (**g**); and 4 healthy human donors from 4 independent experiments (**h**). Each symbol represents one mouse or healthy donor.

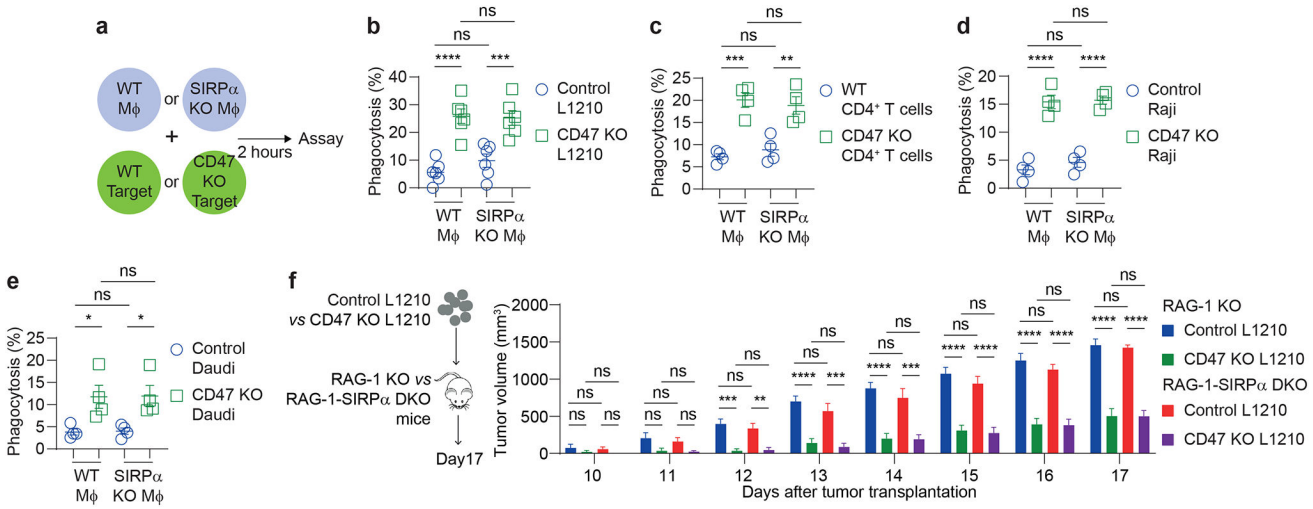

Fig. 2. Genetic deficiency of CD47 or SIRPα phenocopies the differential impact of CD47 or SIRPα blockade.

a-e, Schematic of the phagocytosis assay is shown in (**a**). Phagocytosis of L1210 (**b**), activated CD4$^+$ T cells (**c**), Raji (**d**) and human lymphoma cells Daudi (**e**), expressing or not expressing CD47, by WT or SIRPα KO BMDMs was tested. **f,** As in Fig. 1g, except that control L1210 and CD47 KO L1210 cells were injected sub-cutaneously in RAG-1 KO or RAG-1-SIRPα double (D) KO mice.

All data are means ± s.e.m. ns, not significant; *$p < 0.05$, **$p < 0.01$, ***$p < 0.001$, and ****$p < 0.0001$. Results are pooled from 6 (**b**) or 4 (**c**-**e**) mice studied in independent experiments; 11 (control L1210) or 10 (CD47 KO L1210) mice from 2 independent experiments (**f**). Each symbol represents one mouse.

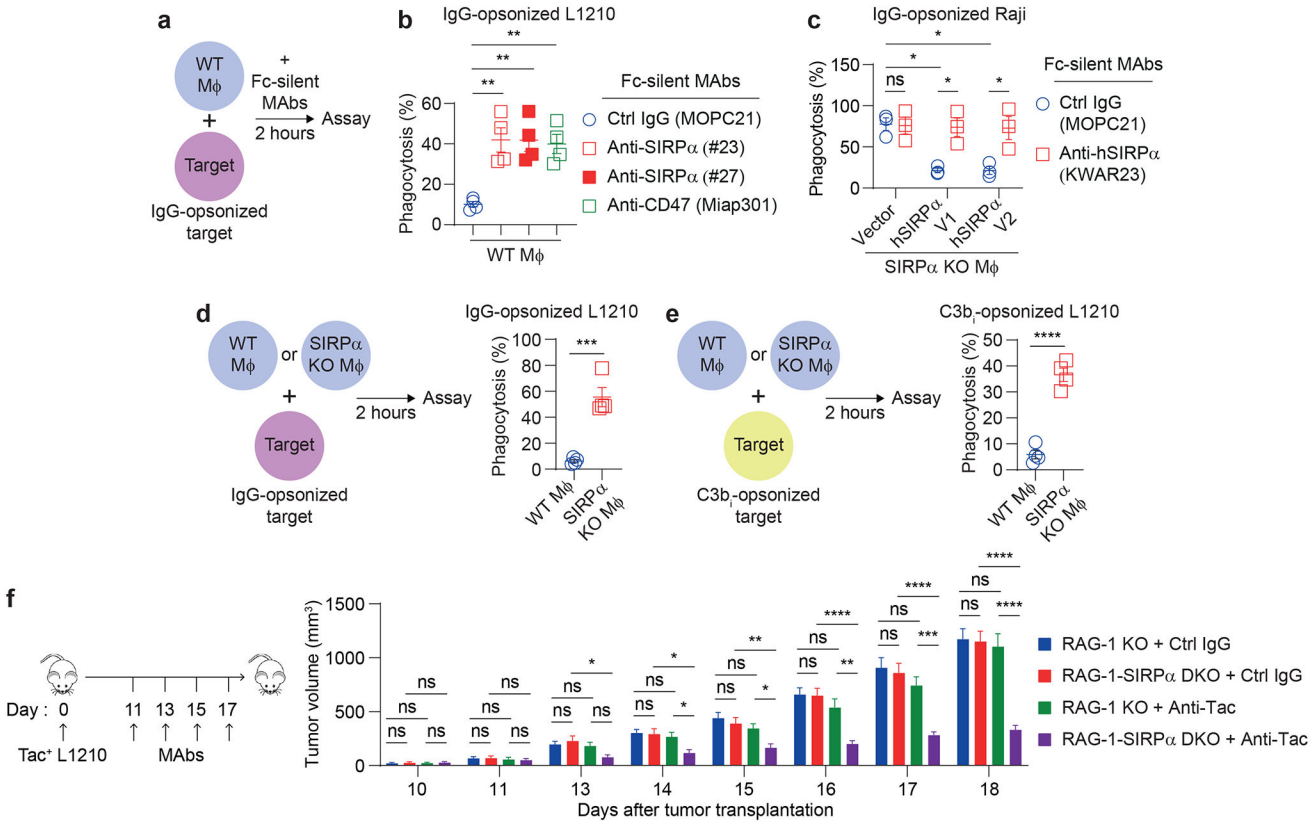

Fig. 3. Blockade or loss of either CD47 or SIRPα promotes phagocytosis of antibody-opsonized tumor cells.

a,**b**, Same as Fig. 1b, except that IgG-opsonized L1210 were used as targets. **c**, Same as Fig. 1h, except that SIRPα KO BMDMs expressing the V1 or V2 variant of hSIRPα and IgG-opsonized Raji were used. **d**,**e,** Same as Fig. 2a, except that IgG-opsonized L1210 (**d**) or $C3b_i$-opsonized L1210 (**e**) were used as targets. **f**, Sub-cutaneous tumor transplantation assay. As in Fig. 1g,2f, except that L1210 derivatives expressing Tac (hCD25) were injected in RAG-1 KO or RAG-1-SIRPα DKO mice. Anti-Tac/hCD25 MAb 7G7, which is a mIgG2a, was used to opsonize the tumor cells.

All data are means ± s.e.m. ns, not significant; *$p < 0.05$, **$p < 0.01$, ***$p < 0.001$, and ****$p < 0.0001$. Results are pooled from a total of 4 (**b**,**d**,**e**) or 3 (**c**) mice studied in independent experiments; 15 mice (16 mice for “RAG-1 KO plus Anti-Tac” group) from 3 independent experiments (**f**). Each symbol represents one mouse.

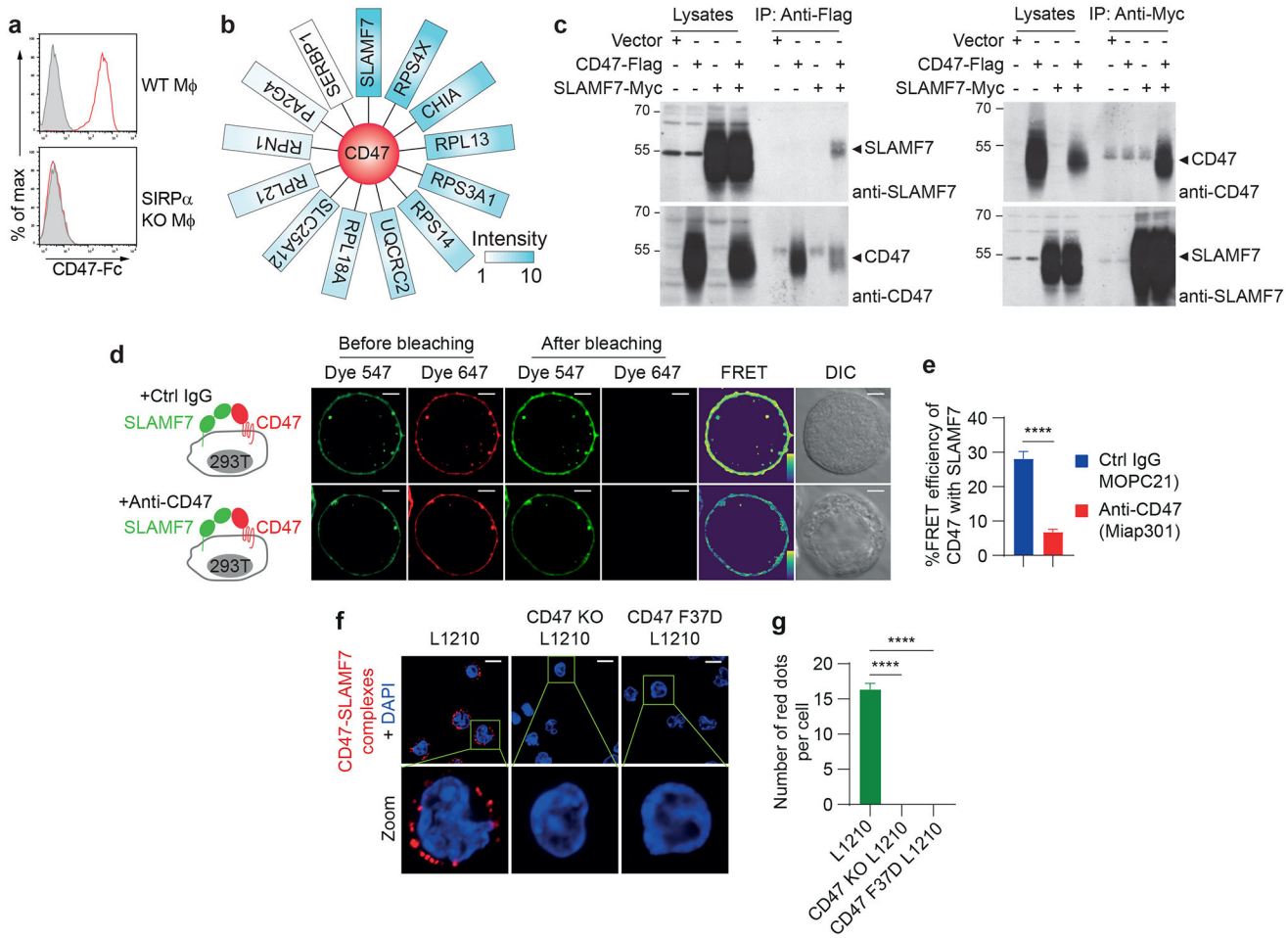

Fig. 4. CD47 physically interacts in *cis* with pro-phagocytic ligand SLAMF7 on tumor cells.

a, Binding of CD47-Fc (red line) to WT or SIRPα KO BMDMs was assayed by flow cytometry. Filled curves, Ctrl Fc. **b,** Mass spectrometry analysis of anti-Flag immunoprecipitates from L1210 cells expressing a Flag-tagged variant of mCD47. The Flag tag was added at the carboxyl terminus of CD47. A schematic representation of the relative abundance, shown with a color gradient, of the various potentially associated proteins is depicted. **c**, Co-immunoprecipitation of CD47 and SLAMF7 in CD47 KO 293T cells expressing a Flag-tagged variant of mCD47 and a Myc-tagged variant of mSLAMF7. Flag and Myc tags were added at the carboxyl terminus of CD47 or SLAMF7, respectively. The abundance of the transfected proteins in total cell lysates was analyzed in parallel. IP, immunoprecipitation. **d**,**e**, FRET assay. (**d**) CD47 KO 293T cells were transfected with tagged versions of mCD47 and mSLAMF7. After coupling the two proteins to different fluorophores (Dye 647 for CD47 as acceptor and Dye 547 for SLAMF7 as donor), proximity was analyzed by FRET, in the presence of the indicated MAbs. Schematic representations of the experimental conditions are depicted on the left, while representative confocal microscopy images are shown on the right. Pre- and post-bleaching confocal images, as well as the calculated FRET efficiency images (pseudo-color; the yellow to purple spectrum denotes strong to weak FRET) and the differential interference contrast (DIC) images, are shown. (**e**) FRET data for 18 independent cells are graphically represented. Scale bars, 5 μm.

(**f**,**g**) Proximity ligation assay (PLA) assay. After cells were fixed, PLA assay was performed according to the manufacturer's recommendations. Representative confocal microscopy images of CD47-SLAMF7 complexes (red dots), in addition to nuclear staining using DAPI (blue), are shown in (**f**), while a quantitation from a total of 100 cells in three experiments is depicted in (**g**). Scale bar, 10 μm. F37D, phenylalanine 37-to-aspartate 37 mutation.
All data are means ± s.e.m. ****$p < 0.0001$. Results are representative of 5 (**a**) or 3 (**c**,**d**,**f**) independent experiments. Results are pooled from 3 (**b**,**e**,**g**) independent experiments.

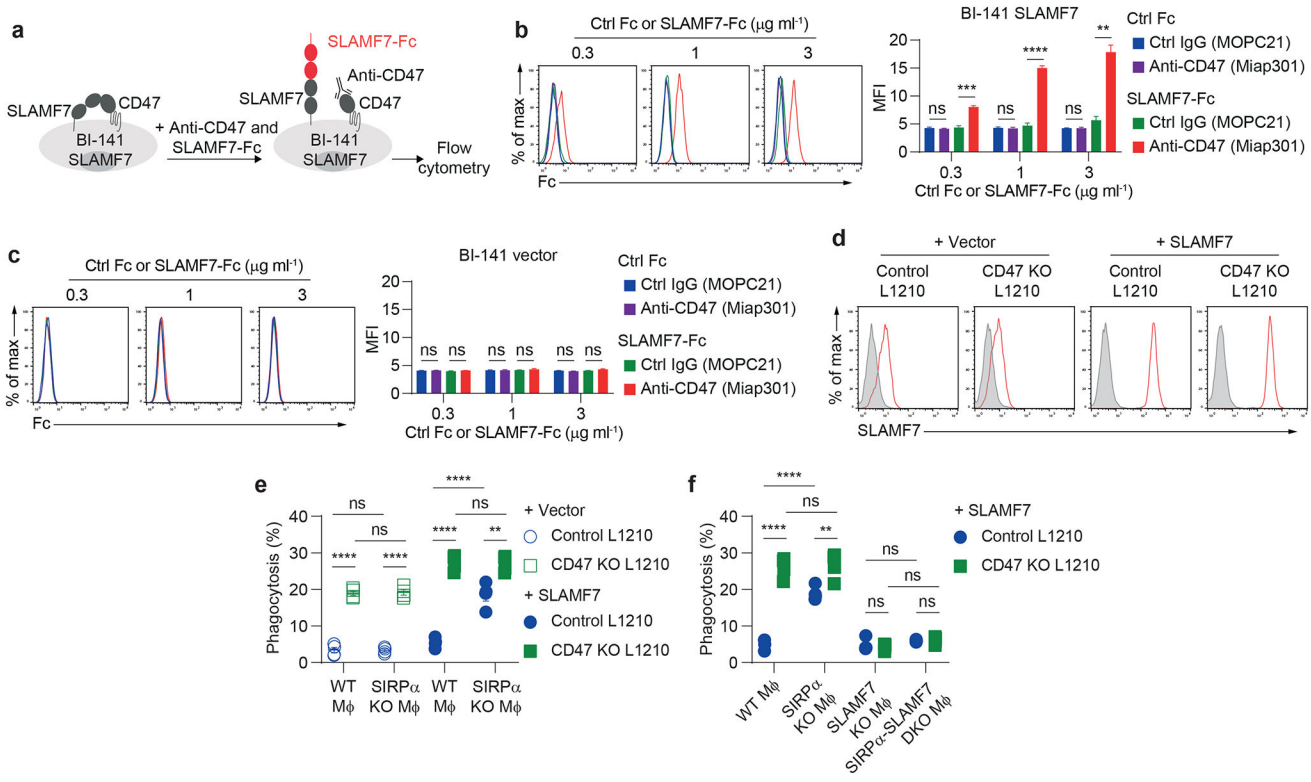

Fig. 5. Freeing of SLAMF7 from CD47 correlates with greater phagocytosis.

a,**b**, The impact of blocking anti-mCD47 MAbs on the ability of mSLAMF7 on tumor cells (BI-141) to interact in *trans* with mSLAMF7 was tested. A schematic representation of the assay is depicted in (**a**). BI-141 cells expressing mCD47 and mSLAMF7 were treated with the indicated MAbs, prior to staining with mSLAMF7-Fc or control Fc fusion proteins. The mean fluorescence intensity (MFI) of fusion protein staining was assayed by flow cytometry. Representative experiment is shown in (**b**, left) and quantification of the data is shown in (**b**, right). **c**, Same as b, except that BI-141 cells without mSLAMF7 expression were used. **d**,**e** Same as Fig. 2a, using control and CD47 KO L1210, with or without mSLAMF7 overexpression, as targets. Expression of SLAMF7 is depicted in (**d**). Red lines, anti-SLAMF7; filled curves, Ctrl IgG. Phagocytosis assays are shown in (**e**). **f**, Same as e, except that WT, SIRPα KO, SLAMF7 KO, or SIRPα-SLAMF7 DKO BMDMs were used. All data are means ± s.e.m. ns, not significant; $^{**}p < 0.01$, $^{***}p < 0.001$, and $^{****}p < 0.0001$. Flow cytometry profiles are representative of 3 (**b**-**d**) independent experiments. Results are pooled from 3 (**b**,**c**) independent experiments; 4 (**e**,**f**) mice studied in independent experiments. Each symbol represents one mouse.

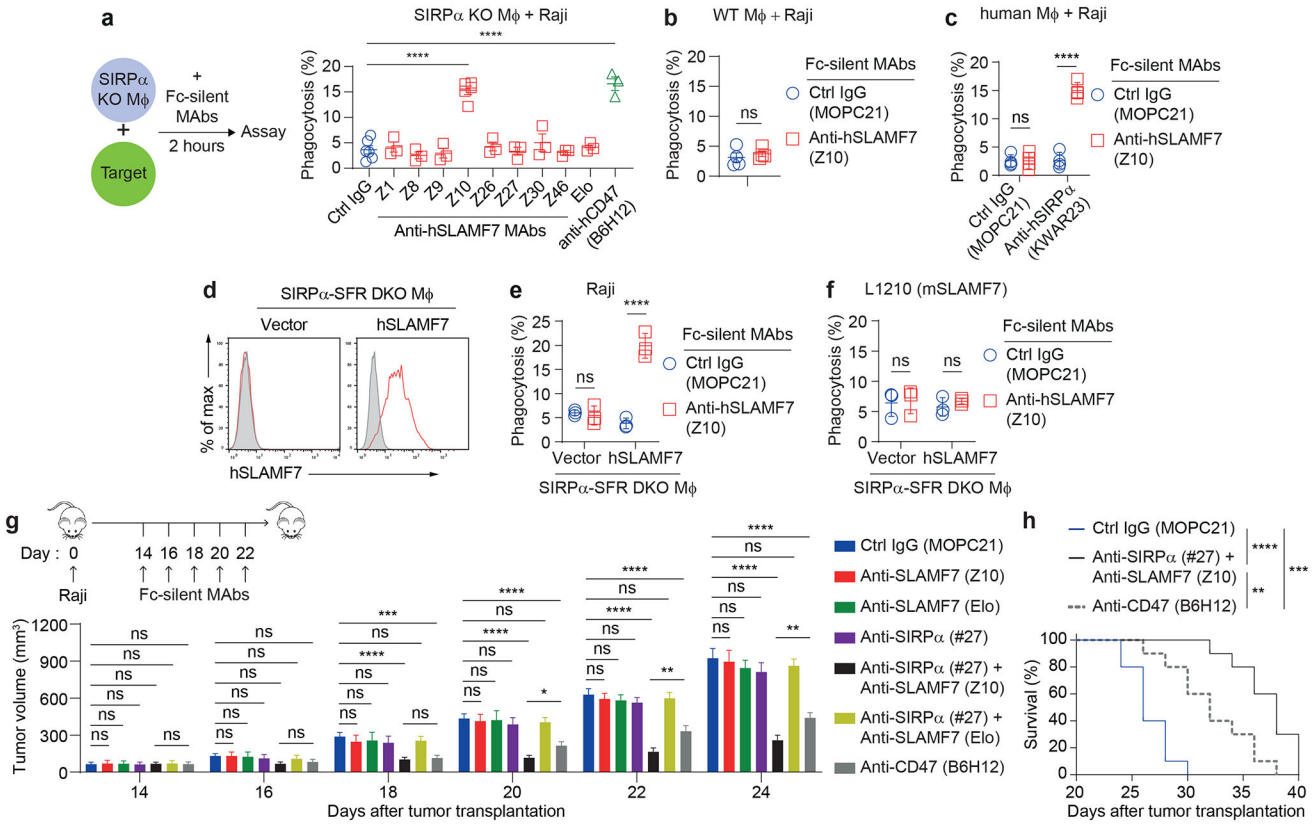

Fig. 6. Identification of a first-in-class anti-SLAMF7 MAb with agonistic activity towards phagocytosis.

a,**b**, Same as Fig. 1b, using SIRPα KO (**a**) or WT (**b**) BMDMs, Raji cells and the indicated MAbs. Elo, elotuzumab. **c**, Same as Fig. 1h, using human macrophages, Raji cells and the indicated MAbs. (**d**-**f**) Same as a, except that SFR-SIRPα DKO BMDMs, expressing or not expressing hSLAMF7 (**d**), and hSLAMF7-positive cells Raji (**e**) and mSLAMF7-positive cells L1210 (**f**) as targets were used. Expression of hSLAMF7 (red lines) was determined by flow cytometry. Filled curves, control IgG. (**g**,**h**) RAG-1 KO mice were injected subcutaneously with Raji, in the presence of the indicated MAbs. Tumor volume over time was measured using a caliper (**g**). Kaplan-Meier plot of survival is shown in (**h**). Elo, elotuzumab.

All data are means ± s.e.m. ns, not significant; *$p < 0.05$, **$p < 0.01$, ***$p < 0.001$, and ****$p < 0.0001$. Flow cytometry profiles are representative of 3 (**d**) independent experiments. Results are pooled from 3 (**a**, except 6 for Ctrl IgG and 5 for Z10) (**e**,**f**) or 4 (**b**) mice studied in independent experiments; 4 healthy human donors from 4 independent experiments (**c**); 18 mice [“Ctrl IgG (mopc21)”, “Anti-SIRPα (#27) plus Anti-SLAMF7 (Z10)” and “Anti-CD47 (B6H12)” groups] from 4 independent experiments, 8 mice [“Anti-SLAMF7 (Elo) and “Anti-SIRPα (#27) plus Anti-SLAMF7 (Elo)” groups] from 2 independent experiments, 7 mice [“anti-SLAMF7 (Z10)” and “anti-SIRPα (#27)” groups] from 2 independent experiments (**g**); 10 mice from 2 independent experiments (**h**). Each symbol represents one mouse or healthy donor.

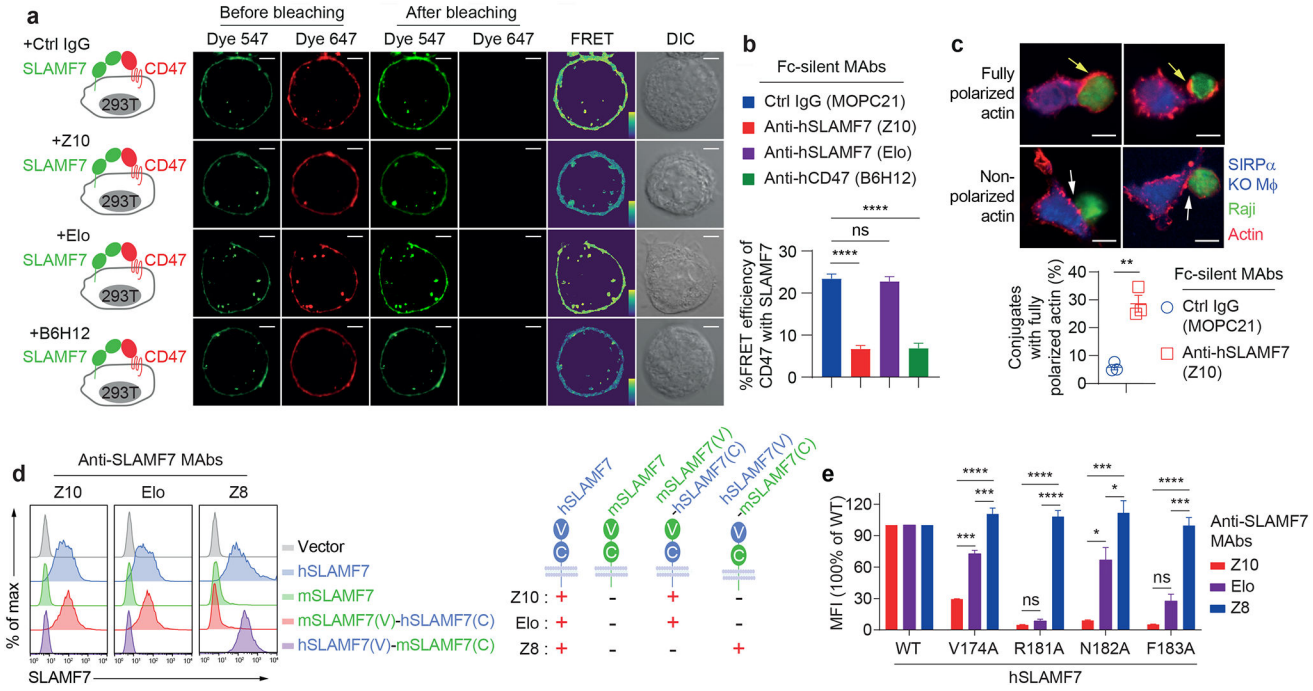

Fig. 7. Agonistic anti-SLAMF7 MAb is a non-blocking antibody that frees SLAMF7 from CD47.

a,**b**, Same as Fig. 4d,e, except that hCD47 and hSLAMF7, in the presence of indicated Fc-silent MAbs, were studied. **c**, Actin polarization in SIRPα KO BMDMs incubated with Raji was detected by immunofluorescence. Top, representative examples of fully polarized (yellow arrows) and non-polarized (white arrows) conjugates. Bottom, quantitation. Scale bars, 5 μm. **d**,**e**, Mapping of the binding sites of MAb Z10, MAb Z8 and MAb elotuzumab (Elo) on CD47 KO 293T cells expressing hSLAMF7, mSLAMF7, chimeras between hSLAMF7 and mSLAMF7, or mutants of hSLAMF7. The mean fluorescence intensity (MFI) of MAbs Z10, Z8 and Elo staining was assayed by flow cytometry (**e**). V, variable Ig-like; C, constant Ig-like; +, binding; -, no binding; WT, wild-type; V174A, valine 174-to-alanine 174 mutation; R181A, arginine 181-to-alanine 181 mutation; N182A, asparagine 182-to-alanine 182 mutation; F183A, phenylalanine 183-to-alanine 183 mutation.
All data are means ± s.e.m. *$p < 0.05$, **$p < 0.01$, ***$p < 0.001$, and ****$p < 0.0001$. Photographs are representative of 3 (**a**,**c**) independent experiments. Flow cytometry profiles are representative of 6 (**d**, except 2 for mSLAMF7) independent experiments. Results are pooled from 3 (**b**,**c**,**e**) independent experiments. Each symbol represents one mouse.